UNIVERSIDADE FEDERAL FLUMINENSE
DEPARTAMENTO DE GEOLOGIA E FÍSICA
PROGRAMA DE PÓS-GRADUAÇÃO EM DINÂMICA DOS OCEANOS E DA TERRA

MATHEUS FERNANDES BORGES SILVA DE PAIVA

ON THE TEMPORAL VARIABILITY OF SALINITY ALONG NEUTRAL DENSITY SURFACES FROM OBSERVATIONAL DATA IN THE SOUTHWESTERN ATLANTIC OCEAN (1998 - 2018)

Niterói, RJ
2021

MATHEUS FERNANDES BORGES SILVA DE PAIVA

ON THE TEMPORAL VARIABILITY OF SALINITY ALONG NEUTRAL DENSITY SURFACES FROM OBSERVATIONAL DATA IN THE SOUTHWESTERN ATLANTIC OCEAN (1998 - 2018)

Dissertação apresentada ao Programa de Pós-Graduação em Dinâmica dos Oceanos e Terra, da Universidade Federal Fluminense, como requisito parcial para obtenção do grau de Mestre.
Área de Concentração: Hidrografia

Orientador: Prof. Dr. Rer. Nat. Andre Luiz Belem

Niterói, RJ
2021

MATHEUS PAIVA

ON THE TEMPORAL VARIABILITY OF SALINITY ALONG NEUTRAL DENSITY SURFACES FROM OBSERVATIONAL DATA IN THE SOUTHWESTERN ATLANTIC OCEAN (1998 – 2018)

Dissertação apresentada ao Programa de Pós-Graduação em Dinâmica dos Oceanos e Terra, da Universidade Federal Fluminense, como requisito parcial para obtenção do grau de Mestre. Área de Concentração: Hidrografia

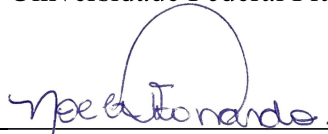Aprovada em 30 de junho de 2021.

BANCA EXAMINADORA

_____

Prof. Dr. Rer. Nat. Andre Luiz Belem (orientador)

UFF - Universidade Federal Fluminense

_____

Dra. Noele Franchi Leonardo

UFF - Universidade Federal Fluminense

_____

Dr. Tiago Segabinazzi Dotto

University of East Anglia (UK)

"o oceano sempre fornece alimento aos filhos e filhas do mar."
Provérbio Yorùbá

odoyá, yèyé omo ejá!

RESUMO

Com extensão aproximada de 8.500 km entre as latitudes 34,5°S e 6°N, a área oceânica adjacente ao Brasil - incluindo a zona econômica exclusiva - é conhecida como "Amazônia Azul", e quando comparada com outras, possui baixo número de observações oceanográficas discretas para os últimos 50 anos. Esta dissertação apresenta um banco de dados hidrográficos, ainda não integrado com os principais bancos de dados oceanográficos internacionais (WOD & GLODAP), sendo um conjunto inédito de 28 expedições oceanográficas da Marinha do Brasil e do PIRATA-BR entre os anos de 1998 e 2018. Perfazendo um total de 783 estações oceanográficas de lançamentos de Rosette/CTD, os perfis atingem profundidades entre a plataforma continental e o oceano profundo (até 5800 m de profundidade), e foram analisados em ampla escala espaço-temporal. Os dados obtidos nas estações oceanográficas foram processados, de acordo com o padrão internacional GO-SHIP, a fim de investigar a estrutura termohalina vertical da coluna d'água, bem como investigar a variabilidade da salinidade ao longo de superfícies de densidade neutra correspondentes às interfaces de massas d'água por duas décadas de observação. Finalmente, os resultados aferidos, além de diminuir o viés espaço-temporal dos dados disponíveis, descrevem uma tendência de salinificação na camada superior (+0,01993; +0,00186 g/kg . ano-1), um dipolo de tendências de dessalinificação-salinificação na camada central (+0,00062; -0,00231 g/kg . ano^{-1}) e águas intermediárias (-0,00155; +0.00042 g/kg . ano^{-1}), e uma tendência de diminuição de salinidade em águas profundas (-0.00043; -0,0016 g/kg . ano^{-1}).

Palavras-chave: estrutura termohalina, variações de salinidade, hidrografia de navio, comparabilidade de dados.

ABSTRACT

With an approximate length of 8500 km between latitudes 34.5°S and 6°N, the ocean area adjacent to Brazil - including the economic exclusive zone - is known as the "Blue Amazon", with an equivalent area of approximately 3.5 million km², but with much less discrete oceanographic observations if compared to other ocean regions in the last 50 years. This study introduces a hydrographic data not yet fully integrated with the main oceanographic databases (WOD & GLODAP), including an unprecedented set of 28 oceanographic expeditions from the Brazilian Navy and PIRATA-BR between the years 1998 and 2018, performing a total of 783 oceanographic stations with Rosette/CTD systems at varying depths between the continental shelf and the deep ocean (up to 5800 m deep) that were not analyzed on such a broad scale before. The data obtained at all oceanographic stations were reprocessed according to the international standard GO-SHIP in order to investigate the vertical thermohaline structure of the water column, as well as to analyze the salinity variability along several neutral density surfaces corresponding to water masses interfaces throughout the last two decades. Finally, the observed results depict a salinification trend in the upper layer (+0.01993; +0.00186 g/kg . yr^{-1}), a dipole of freshening-salinification trends in central (+0.00062; -0.00231 g/kg . yr^{-1}) and intermediate waters (-0.00155; +0.00042 g/kg . yr^{-1}), and a freshening trend in deep waters (-0.00043; -0.0016 g/kg . yr^{-1}), which diminishes the spatio-temporal aliasing of available discrete data and secures even more robustness for inferences in the Southwestern Atlantic Ocean.

Keywords: thermohaline structure, salinity change, ship-based hydrography, data comparability.

LIST OF FIGURES

LIST OF TABLES

LIST OF ACRONYMS

AABW – Antarctic Bottom Water

AAIW – Antarctic Intermediate Water

AMOC – Atlantic Meridional Overturning Circulation

BC – Brazilian Current

BNDO – Brazilian National Oceanographic Database

CTD – Conductivity-Temperature-Depth

GLODAP – Global Ocean Data Analysis Project

GO-SHIP – Global Ocean Ship-based Hydrographic Investigations Program

NBC – North Brazil Current

ODV – Ocean Data View® software

PIRATA-BR – Prediction and Research Moored Array in the Tropical Atlantic Project (Brazil)

QC – Quality Check

NADW – North Atlantic Deep Water

SACW – South Atlantic Central Water

TEOS-10 – Thermodynamic Equation of State of Seawater

T-S – Temperature-Salinity

TW – Tropical Water

WOD – World Ocean Database

CONTENTS

1. INTRODUCTION

Properties of water in the ocean are not uniformly distributed so that different regions and depths (or densities) are characterized by different coefficients or ranges of attributes such as temperature, salinity, density, oxygen, and nutrients. The spatial distribution and variability over time of thermohaline characteristics through the water column mainly rule several oceanographic features, especially in the large-scale circulation as well as registering effects of modern climate changes in ocean heat content (e.g. Azar et al., 2020; Palmer et al., 2019; Barlett et al., 2017; Poole and Tomczak, 1999).

Parcels of water with similar properties often share a common formation history and are referred to as water masses or source water types. In general, the vertical and horizontal mixing of various water masses advected into an area define ocean stratification. Since temperature and salinity are considered to be 'conservative properties' these characteristics would slowly modify as the water mass is advected downwards to the subsurface, being only changed at the sea surface or by mixing but not consumed over time. Hence, the T-S relationship constitutes a key proxy to track the circulation and mixing of water masses (Emery, 2001). Recently, evolution of observational capacities has been allowing the investigation of new physical and chemical parameters related to the definition of water masses and their boundaries, such as internal energy, entropy, enthalpy, potential enthalpy, and chemical potentials of seawater (Todd et al., 2019; Palmer et al., 2019; Souza et al., 2018; Ferreira and Kerr, 2017; McDougall et al., 2013). Since the gradient configuration is a major driving force on the circulation and mixing of the oceans, most physical oceanography studies are dependent on the density of seawater; therefore, the more accurate we estimate salinity and density, right from temperature-conductivity-pressure discrete measurements, the more realistic new analysis and models will be.

Research vessels and ships of opportunity have been the primary approach of observing oceanographic features such as currents and water masses systems for a prolonged time. Ship-based hydrography can measure many Essential Ocean Variables, through the full water column being uniquely capable of collecting multiple types of samples spanning physical, biogeochemical, and biological/ecosystem methods with equivalent reference standards, high-quality and high-resolution reach. Adversely, some of the principal limitations on research vessels' contribution to sustained ocean observing are their high operation budgets and the irregularity of cruises (Todd et al., 2019).

Brazil has settled multiple policies on oceanographic data via the Directorate of Hydrography & Navigation, such as the Oceanographic Data Collection Plan, which intends to manage data interchanges with other institutions under the Intergovernmental Oceanographic Commission of the United Nations scope. Parallel to that, the BNDO has been compiling information and datasets acquired from ship-based methods in Brazilian waters by the whole international and national communities in the last decades. In the context of the Worldwide Met-Ocean Information and Warnings Service, Brazil is responsible to elaborate and share meteorological forecasts and bad weather alerts in the region called METAREA V: Atlantic waters west of 20°W from 35°50'S to 7°N, narrowing in the coastal strips at the extremities to the Uruguay/Brazil frontier in 33°45'S and the French Guyana/Brazil frontier in 4°30'N (Fig. 1). The METAREA V comprises both Brazilian and international waters, including the western limb of the AMOC, so the investigation and monitoring of processes and features within this area is crucial for advances in science and governance. This dissertation is focused on observational data acquired within METAREA V from 1998 to 2018.

The Atlantic Ocean, through the AMOC, has a striking influence on global climate and distribution of heat content. Consisting of a double cell of a northward flow of upper

ocean waters that become denser in the northern North Atlantic and flow out southward at depth, eventually becoming NADW, and a northward flow of dense AABW that upwells into the lower part of the NADW, disappearing by the mid-latitude North Atlantic (Talley, 2011). Temporal and spatial variability in ocean heat storage is linked to decadal varying atmospheric forcing and the spatial pattern and variability of the ocean's overturning circulation (Talley et al., 2016). The strength of the AMOC is believed to have been extremely reduced in past ages due to extreme climate changes (e.g., glacial and deglacial periods), even interrupting the process of deep water formation (Marson et al., 2014).

Time-limited in situ observations and model uncertainties still make it difficult to separate natural from anthropogenic long-term AMOC variability. From models, Hirsch and Marotzke (2007) noted a high frequency of variability in AMOC, which could produce false trends in the analysis of small temporal scales. Rayner et al. (2011) also observed the existence of a strong seasonal pattern in AMOC transport, yet it should be better understood.

Within METAREA V, the water column can be divided into five major water masses: Tropical Water (TW); South Atlantic Central Water (SACW); Antarctic Intermediate Water (AAIW); North Atlantic Deep Water (NADW); and Antarctic Bottom Water (AABW); each one represented by a T-S index and summarized in Table 1, according to the references cited.

Table 1. Water mass nomenclature, acronyms, and temperature-salinity coefficients/ranges in the South Atlantic as defined by the references cited.

Acronym	Water Mass	Section	Conservative Temperature (ºC)	Absolute Salinity (g kg⁻¹)	References
TW	Tropical Water	Tropical	> 26	< 36.5	Stramma & England (1999); Costa da Silva et al. (2021)
		Subtropical	> 18.5	> 36	Campos et al. (1995)
SACW	South Atlantic Central Water	Tropical	6.55 - 20.0	34.9 - 36.2	Poole & Tomczak (1999); Costa da Silva et al. (2021)
		Subtropical	6 - 18.5	34.5 - 36.0	Campos et al. (1995)
AAIW	Antarctic Intermediate Water	METAREA V	2 - 5.98	33.97 - 34.98	Almeida et al. (2018); Emery (2001)
NADW	North Atlantic Deep Water	METAREA V	1.49 - 3.98	34.95 - 35.16	Almeida et al. (2018); Garzoli et al. (2015); Koltermann et al. (2011)
AABW	Antarctic Bottom Water	METAREA V	< 1.68	< 34.7	Almeida et al. (2018); Emery (2001)

In the upper 1500 meters, the circulation is mainly linked with wind forcing through Ekman pumping and subduction which makes the surface and sub-surface circulation even more subtle (Barberini, 2017). Beyond the energetic wind-driven regime in the upper column, circulation below the pycnocline may be mostly associated with currents flow, buoyancy forcing, and overturning circulation. This includes weaker flows that are easily masked by eddies dynamics and the Deep Western Boundary Current present at all latitudes in the Atlantic (Talley et al., 2011).

Additionally, the METAREA V presents peculiar oceanographic characteristics. Within the Tropical section, the NBC exports waters from the south to the north, integrating part of the AMOC (Bower et al., 2019), so while it advances along the continental shelf-slope boundary, the NBC can retroflect feeding eastward currents (more intense in the austral

summer and fall), or continue its path northwestwards (Urbano et al., 2006; Dorfschäfer et al., 2020).

Thereabout the Subtropical section of METAREA V, the region is notable by its strong mesoscale activity in the form of meanders and eddies mainly associated with the BC southwards flow bordering the continental shelf-slope boundary (Campos et al., 1995). In the vicinity of Cabo de São Tomé and Cabo Frio, with the abrupt change in the direction of the coastline, by inertia, the BC continues to move to deeper regions while changes on potential vorticity of the current generate a series of meanders and mesoscale eddies. This fact in synergy with the baroclinic instability generated by the shear between BC and Intermediate Western Boundary Current has a great impact on local dynamics (Dorfschäfer et al., 2020). Further south, the thermohaline structure of the Brazil-Malvinas Confluence ($35 \sim 40^{\circ}$S) is marked by an intense temperature and salinity gradient. On the western boundary along the front formed in the confluence zone, there is an intrusion of waters with very low salinity reminiscent from the plumes of La Plata River and Patos Lagoon, which can be advected to the north by the Malvinas Current and the BC retroflection (Dorfschäfer et al., 2020).

There are various previous works, which will be presented for discussion, describing changes and variabilities through the whole water column in the South Atlantic over recent decades. According to Bindoff and McDougall (1994), salinity changes at depth have two main causes: (i) changes on isopycnals (freshening/salinification or warming/cooling) without changes in density; or (ii) heave, which is related to vertical displacements of isopycnals and thus a change in density, temperature and salinity. Therefore, knowledge of these salinity changes requires understanding the causes of density changes at intermediate levels.

In this study, TEOS-10 and GO-SHIP standards were elected to be used as the "gold standard" of available practices for subsurface observations, data processing and analysis

5

(Palmer et al., 2019; Almeida et al., 2018). TEOS-10 supersedes the old equation of state of seawater EOS-80 which has been in place for 30 years, bringing many important advantages on the representation of thermodynamic properties of seawater, as well as facilitating the development of salinity estimation technologies and long-term stability to better investigate climate change processes. For most purposes in which observational data are analyzed, the Absolute Salinity S_A (g . kg^{-1}) and Conservative Temperature Θ (ºC) are the appropriate salinity and temperature variables, respectively, to be used in situations of turbulent mixing, T-S plots, and determination of the characteristics of water masses and their mixtures, instead of the older Practical Salinity and Potential Temperature (Pawlowicz, 2010).

S_A is the salinity output of the TEOS-10 algorithms which considers the spatially varying composition of seawater and addresses all the thermodynamic properties of seawater. Concomitantly, Θ represents the heat content of seawater more accurately than the older potential temperature does, despite being closer (by a factor of a hundred) to a conservative variable than the former (Pawlowicz, 2010). Mathematically simplifying, it is the potential enthalpy divided by the fixed heat capacity of seawater. From that, lateral heat diffusion along neutral tangent planes can be more than 1% different when estimated using gradients of potential temperature rather than Conservative Temperature (Pawlowicz, 2010).

Furthermore, to smooth out some of the higher frequency variability (i.e. mesoscale eddies and internal waves), the investigation of halocline variation should be along neutral density surfaces (McCarthy et al., 2011; McDougall, 1987). The neutral density, denoted by γ_n, is a function of salinity, in situ temperature (°C), pressure (db), and latitude/longitude position. Surfaces of constant γ_n depict the neutral surfaces, along which the strong lateral mixing occurs in the ocean, and across which the mixing is determined by the vertical small-scale diffusivity. As such, γ_n surfaces provide an appropriate vertical coordinate for understanding the ocean circulation, once it is all the more linked to a global hydrographic

dataset (Levitus, 1982 *apud* Jackett and McDougall, 1997). Neutral densities are the continuous analog of discretely defined and locally referenced potential density surfaces while having better accuracy (up to a factor of 5) and simpler calculation, assigning it as a very efficient method of quantitatively describing isopycnal mixing (Jackett and McDougall, 1997).

A series of improvements have been achieved with the use of a neutral framework in the diagnosis and analysis of water masses processes. As discussed by McDougall (1987), the former isopycnal framework does not allow considering surface and interior transformation processes at the same time, which leads to problems in identifying water masses below 500 m because the isopycnal is not tangent to the neutral surface. The use of this global density variable, named neutral density, supports the expansion of classical methods of estimating water-mass transformation using surface fluxes (Tziperman, 1986) to the whole oceanic domain. Additionally, the Ocean General Circulation Model applications have also shown that the use of a neutral density framework is more adequate when dealing with thermodynamics of the global thermohaline circulation (Iudicone et al., 2008).

The ocean salinity distribution is set by the transport of freshwater through the ocean and atmosphere. Variations in the hydrological cycle and cryosphere are the leading causes for large-scale salinity change (Talley et al., 2016). In the South Atlantic, salinity changes are depth and latitudinally dependent, presenting the most significant variation in the upper 500 m of the water column because of direct atmospheric influence (Curry et al., 2003). Furthermore, changes in temperature and salinity in deep waters are an expressive signal from overall changes in ventilation rates and properties of the waters that fill mostly global abyssal basins.

Several studies have focused on changes within defined water masses layers or neutral density surfaces. Thus, some uncertainties have arisen from observational and modeling results.

Significant differences in salinity between ocean basins are apparent, especially the relatively higher salinities of the upper Atlantic Ocean when compared to the Pacific and Indian oceans. In part, this difference is due to the continental distribution along ocean basins, which the narrow Atlantic basin contributes to higher evaporation rates and consequently higher salinity values since a larger portion of its surface is under influence of continental dry air (Belem et al., 2019).

From the mid-90s, quality controlled oceanographic profile salinity measurements from the World Ocean Database 2001 have shown salinity increases in the upper column of tropical-subtropical latitudes due to warming and increased evaporation, with the largest salinity increases occurring between 20°S and 20°N, being up to +0.003 year^{-1}, yet subject to intense interannual and decadal variability (Durack & Wijffels, 2010; Boyer et al., 2005; Curry et al., 2003). Zhu & Liu (2020) show a remote response of the AMOC slowdown detected in the South Atlantic by a salinity indicator called the Atlantic 'salinity pile-up'. This salinity indicator differs from the traditional 'salty-getting-saltier' fingerprint in the global sea surface salinity identified in observations and models and refers to a relatively greater trend in basin-mean salinity increase in the subtropical Atlantic, also up to +0.003 year^{-1} from observational data, than the Indo-Pacific from the surface to the thermocline (>300 to 500m). This salinity pile-up was detected in observation and model ensembles for both the historical period and future warming scenarios.

At the intermediate layer, several previous studies have identified warming and salinification associated with the AAIW in the Atlantic Basin (Bindoff and McDougall, 1994; Arbic and Owens, 2001; Boning et al., 2008; Schmidtko and Johnson, 2012; Goes et al.,

2014). These studies almost uniformly find warming and salinification with passing time on isopycnals denser than the AAIW salinity minimum and usually (although not always) note a cooling and freshening overtime on lighter isopycnals. This isopycnal cooling and freshening above the AAIW and warming and salinification below form a dipole around the core of the AAIW (Schmidtko & Johnson, 2012). Advection in the intermediate water layer by the transport along the western boundary plays a dominant role in the variability of AAIW salinity (Fu et al., 2019). As a salinity minimum, AAIW becomes more saline on the way of northward spreading, due to mixing with surrounding waters (Fu et al., 2019). A stronger (weaker) western boundary transport would carry more (less) fresher AAIW from the South Atlantic to the tropics, affecting the local salinity at intermediate depth (Fu et al., 2019). Although long‑term warming and salinification trends have been assessed, it remains unclear whether AAIW properties also vary on interannual timescales since different works have achieved contradictory trends. McCarthy et al. (2011) showed that the AAIW core salinity in the South Atlantic varies on interannual timescales with a peak-to-trough magnitude of 0.06 and attributes that to westward propagation of planetary waves. Differently, Curry et al. (2003) and Yao et al. (2017) have observed a basin-scale freshening trend in the AAIW percolating the southwestern Atlantic, up to -0.003 year^{-1}, while this freshening in the intermediate water layer is thought to be compensated for by increased salinity in shallower thermocline water, indicating a contemporary intensification of the hydrological cycle.

Deeper down, Talley (2008) has observed a NADW freshening trend due to net precipitation and runoff in the Arctic and subpolar North Atlantic. Additionally, Purkey & Johnson (2013) have noted a robust freshening owing to water-mass shifts near the AABW source regions, reaching -0.0005 year^{-1}, and following the path of AABW deep circulation in the three southernmost basins (Atlantic, Pacific, and Indian oceans), reflecting the advection of a fresher variety of AABW into the deep Southern Ocean. Swift & Orsi (2012) as well as

Katsumata et al. (2015) have observed salinity decreases of about -0.003 year^{-1} (a change of -0.06 over two decades) in the Ross Sea and Adélie Land offshore adjacent waters, just on some of the AABW formation areas.

Hence, further investigation of water mass dynamics and available data is needed to better support transdisciplinary analysis and climate/ocean modeling, while observations and equipment are evolving. This work compares three different datasets, one of them unique, to investigate the temporal variability of salinity through the water column for the South Atlantic Ocean.

Sustained ocean data is an essential requirement for assessing the implementation of the United Nations Agenda 2030 and its 17 Sustainable Development Goals, particularly the 14th, in order to "conserve and sustainably use the oceans, seas and marine resources for sustainable development". Governments, policymakers, and every social actor/stakeholder are facing intricate agreements and decisions that demand sustained ocean observations and adoption of open data policies, while the global reality is still deficient in both observations and the necessary integration. In many oceanic regions, sustained data acquisition is too sporadic, sparse, inadequate, or imprecise. The improved understanding of the ocean dynamics achieved in the past decades, aligned with the recognition of our needs for continued observation, analysis, investigation, and prediction of oceanic features and processes will support the returns of this important societal investment (Tanhua et al., 2019).

Tanhua et al. (2019) bring yet the main elements of an ocean observing framework integrated with the Global Ocean Observing System, tracing the information paths from inputs (Essential Ocean Variables) to processes (observations and maintenance), to outputs (data and products). The basic characteristics of the framework are the acquisition of EOV and their requirements, common methods of data management and information products, the

readiness levels of data, the incorporation of both coastal and open observations, as well as feedback loops addressing science challenges and social needs.

The goal of this dissertation is to investigate the salinity variability and trends along several neutral density surfaces, from 1998 to 2018, in the Southwestern Atlantic, based on three different datasets. For this purpose, a novel dataset from 39 oceanographic cruises was processed, analyzed, and compared to the WOD18 and GLODAP ancillary datasets. Interannual salinity variability means, and trends of several neutral density surfaces, over Tropical and Subtropical Atlantic, are assessed. Combined statistical and visual analysis of T-S plots, isosurface maps, trend charts, and histograms, for each section, were performed through the ODV software (Schlitzer, 2018).

The dissertation is outlined as follows: data and methods are delineated in Section 2, where the data sources are presented along with the criteria used for data investigation, quality check, and determining the salinity variability along neutral density surfaces; results are presented and discussed in Section 3; this is followed by conclusions and closing remarks in Section 4.

2. DATA AND METHODS

To better assess data representativity and obtain relevant estimates for such a large domain as METAREA V, it has been divided into two major sections: (i) Tropical, from latitude 7ºN to 15ºS; and (ii) Subtropical, from latitude 15ºS to 35ºS, as shown in Figure 1.
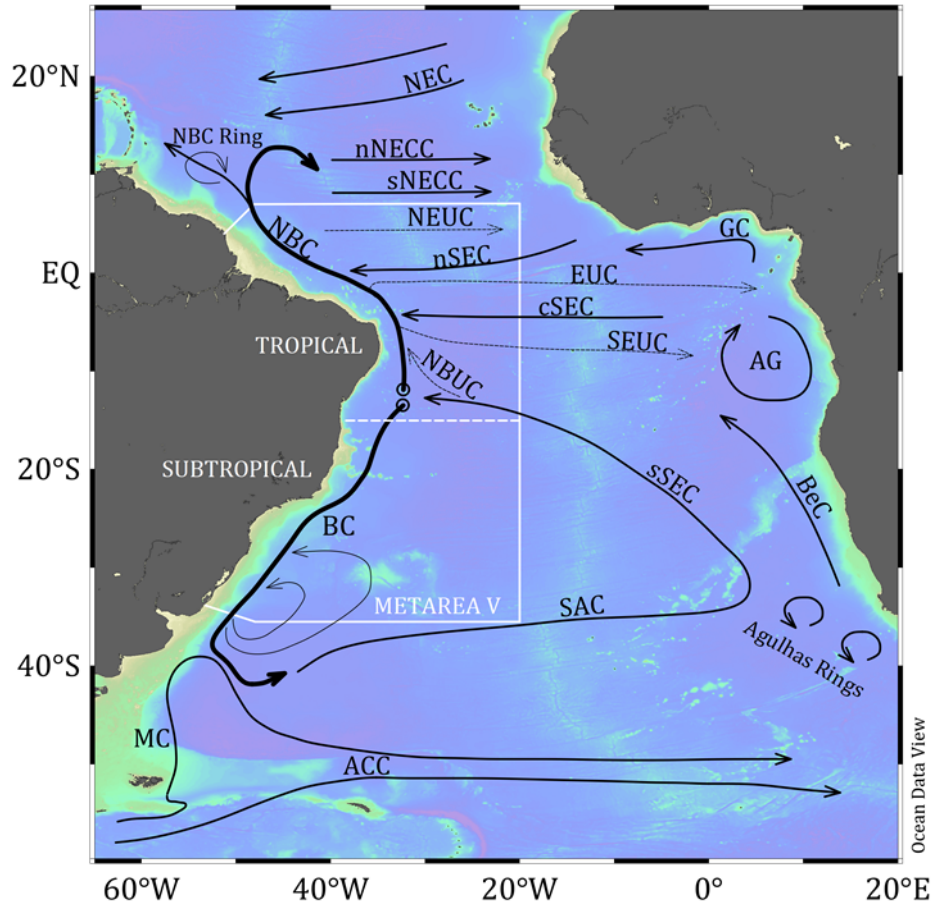
Figure 1. Main oceanographic features present in the South Atlantic. The solid white line delimits the METAREA V region. The dashed white line at 15ºS bisects METAREA V into Tropical and Subtropical sections. Dashed black lines indicate undercurrents while solid lines represent superficial features. BC and NBC are shown in bold lines as the major western boundary currents. Other features outside METAREA V are shown including Malvinas Current (MC), Antarctic Circumpolar Current (ACC), South Atlantic Current (SAC), South Equatorial Current (SEC), Benguela Current (BeC), North Brazil Undercurrent (NBUC), South Equatorial Undercurrent (SEUC), Angola Gyre (AG), North Equatorial Undercurrent (NEUC), North Equatorial Countercurrent (NECC), North Equatorial Current (NEC), and Guiana Current (GC). Adapted from Stramma & England (1999) and Talley (2011).

Neutral density layers were defined based on the literature to examine how salinity has been varying at each water mass boundary. For similar purposes, Herrford et al. (2017) and Hummels et al. (2015) adopted neutral density values to divide the water masses stratification in the latitudinal range from 10ºN to 15ºS, based on the potential density values

presented by Schott et al. (2005). These values are used in this study for examining the Tropical section, while for the Subtropical section, the selected neutral density layers are slightly different, following Azar et al. (2020), Goes et al. (2014), and Preu et al. (2012). Defined neutral density boundaries are shown in Table 2.

Table 2. Defined neutral density surfaces (γ_n) for boundaries between water masses in both *Tropical* and *Subtropical* sections. Adapted from Herrford et al. (2017); Hummels et al. (2015); Azar et al. (2020); Goes et al. (2014); and Preu et al. (2012).

Neutral Density Surfaces γ_n (kg/m^3)		
Water Mass Boundaries	**TROPICAL (7ºN - 15ºS)**	**SUBTROPICAL (15ºS - 35ºS)**
TW - SACW	24.5	26.2
SACW - AAIW	26.8	27.1
AAIW - NADW	27.7	27.6
NADW - AABW	28.135	28.10

2.1 Hydrographic Data Sources

A unique novel dataset acquired during 39 oceanographic surveys in the context of Brazilian Navy Oceanographic Cruises and PIRATA-BR expeditions from 1998 to 2018 is presented. Such oceanographic cruises are conducted mainly for scientific research objectives but also for navy training on data acquisition and engaging human resources from many oceanography institutions over the country. Data access is made through the BNDO (available on-demand) and the PIRATA-BR database (available at http://pirata.ccst.inpe.br). For this study purpose, both BNDO and PIRATA-BR datasets were merged and mentioned hereafter as BNDO in order to assess its distinctiveness from the main international repositories that allow open and ready-access data.

Ancillary data was gathered from the WOD18 (Boyer et al., 2019) of the National Oceanographic Data Center and also from the GLODAPv2.2020 (Olsen et al., 2020) in the same region and period. Temperature and Salinity profiles collected between January of 1998 and December of 2018 at the METAREA V region, extending from 35°S to 15°N and from 30°W to 60°W, were employed in this study (Fig 3).

All datasets used herein assemble vertical profiles acquired mostly from high-resolution CTD casts, as well as from Ocean Station Data, reversing thermometers, bottles and low-resolution CTD. Before being analyzed, the whole dataset has passed through processing and quality check steps that have filtered out non-reliable measurements.

Originally, the BNDO dataset had 1952 raw T-S profiles from 39 cruises scattered within the METAREA V between the years of 1998 and 2018. From the ancillary dataset composed by WOD18 and GLODAPv2.2020, 3244 profiles were accessible for the same arrangement.

2.2 Data Preprocessing & Quality Control

The process of acquiring quality oceanographic data starts prior to the cruise planning and takes a multi-step process before achieving the final product, such as a reliable CTD profile. First, it is important to note that data from this novel dataset was acquired using the CTD equipment from Sea-Bird Electronics (SBE) 911plus. The CTD is equipped with a centrifugal pump and high-resolution sensors for conductivity measurements (resolution = 0.00004 S/m), temperature (resolution = 0.0002 °C) and pressure (resolution = 0,068 db).

Basic QC on data usually scrutinizes for inaccuracy in ship identification, date, location, value, digital encoding, or stuck values, based on global criteria. Other strategies

focus on the temporal and spatial consistency of data subsets. Regular tests on temperature/salinity data identify frozen measurements or acute changes in time series, as well as spikes, unrealistic gradients, or density inversions in vertical profiles. Possible horizontal inconsistencies are often addressed through comparison with local statistics from a climatological ancillary dataset (such as the WOD and GLODAP) verifying that a given discrete measurement lies within a coherent range. The principal aim during QC is to both increase the detection of bad data and reduce misled rejection of good data (Gourrion et al., 2020).

As follows, raw data was processed before interpretation. The processing steps aim to obtain a consistent, spike-free data set. In this context, the GO-SHIP program provides necessary international coordination and scientific oversight for repeat hydrography, including orientations for acquiring and processing several types of oceanographic data, for instance, CTD profiles (Sloyan et al., 2019). "GO-SHIP" refers to the global hydrographic observations with modern standards that began with the World Ocean Circulation Experiment in the 1990s, being afterward incorporated into the Global Climate Observing System and the Global Ocean Observing System.

Hence, according to the GO-SHIP standards (McTaggart & Johnson, 2010), the SBE Data Processing software (version 7.26.7.1; Sea-Bird Scientific, 2017) was used as an initial tool to process the whole CTD dataset. The procedure consists of a standard suite of processing modules from the software in the following order (Fig. 2): "*Data Conversion*", "*Align CTD*", "*Bottle Summary*", "*Wild Edit*", "*Filter*", "*Cell Thermal Mass*", "*Loop Edit*", "*Derive*", "*Bin Average*", and "*Translate*".
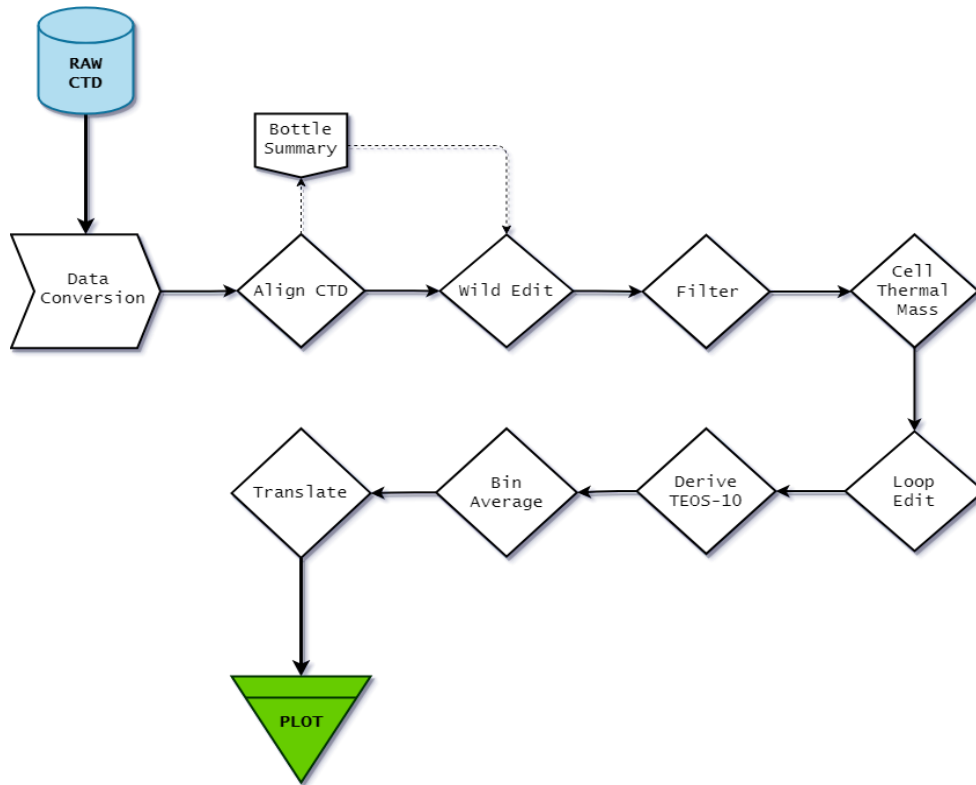
Figure 2. CTD data processing flow chart according to GO-SHIP standards (adapted from McTaggart & Johnson, 2010).

'*Data Conversion*' converts raw data from '.hex' or '.dat' format to '.cnv' engineering units. Both down and upcasts are processed for scan number, elapsed time (s), pressure (dbar), primary temperature (°C), secondary temperature (°C), primary conductivity (mS . cm^{-1}), secondary conductivity (mS . cm^{-1}), and oxygen voltage (when available).

For every plumbed configuration of temperature, conductivity (and oxygen) sensors on the underwater equipment, an alignment in time relative to pressure should be applied to conductivity to reduce salinity spiking when measuring high-gradient isolines. It is not necessary to align temperature, as it is the first sensor to see a parcel of water, but aligning conductivity assures that derived parameters such as salinity and density are estimated using measurements from the same parcel of water. When available, the V1 deck unit aboard, which communicates in real-time with the CTD, automatically advances primary conductivity by 0.073 seconds. Checking the salinity traces for spikes in high-gradient

parcels of water and making minor adjustments to the alignment times, using '*Align CTD*' for each temperature-conductivity sensor pair, is a valuable approach to minimize most salinity spikes.

The '*Bottle Summary*' step is performed when Niskin bottles are launched into the Rosette/CTD to collect water samples. The sensor measurements can be used along with sample data to calibrate the equipment and accordingly correct acquired profiles. It can also be used to average upcast data and derive primary and secondary salinity, potential temperature, potential density anomaly, and dissolved oxygen concentration (μmol kg^{-1}).

'*Wild Edit*' is used to remove extreme outliers by scanning twice the data in bin batches. The first pass flags points that are greater than 2 standard deviations from the mean of the respective bin. The second pass estimates a new mean and standard deviation from these previously flagged points and removes measurements greater than 20 new standard deviations from the latest mean.

'*Filter*' can be used to smooth some of the digitization noise in pressure by applying a low pass filter to pressure, generally with a time constant four times greater than the CTD acquisition rate. In order to produce a zero-phase (no time shift) record, the filter is first run forward through the file and then run backwards.

Once the conductivity cell is located downstream of the thermistor in an SBE 911plus CTD, and it exchanges heat with water passing through it, the temperature of a parcel of water is inevitably different between the conductivity cell and the thermistor. '*Cell Thermal Mass*' thus uses a recursive filter to alleviate cell thermal mass effects from measured conductivity.

"*Loop Edit*" identifies deceleration or reversal in pressure measurements and flags those spurious measurements caused mainly by the ship's play at sea (heave, roll, pitch). Optionally, the "Loop Edit" step can also mark values associated with disturbances of surface to delete or just flag invalid data.

'*Derive TEOS-10*' uses the primary pressure, temperature, and conductivity measures to compute secondary variables such as depth, neutral density, absolute salinity, conservative temperature, dissolved oxygen, sound speed, as well as any other desired parameter using TEOS-10 formulas.

'*Bin Average*' averages the sensor-response corrected 24-Hz data into predefined bins related to a chosen variable such as pressure/depth (most used), time, or number of scans. Each bin is centered on an integer pressure value, e.g. the 1-dbar bin average scans where pressure is between 0.5 dbar and 1.5 dbar. Once for all, '*Translate*' converts the binary data file to ASCII format.

Final converted data was then checked for metadata integrity: incoherent/missing latitudes, longitudes, time, and dates. Questionable values were compared with adjacent profiles and cruise reports to make sure that discrepancies were not introduced during the conversion process. Upon completion of these preliminary quality control checks, the dataset was imported into ODV software (Schlitzer, 2018) where only downcast profiles were selected for the analysis.

Extensive duplicate checks were performed – first internal to the new dataset, and then the data was checked against the ancillary WOD18 and GLODAPv2.2020 databases. Duplicates are a continuous problem with any historical database since each repository treats metadata in its standards, which can further difficult the identification of duplicate stations. Duplicate checks include identifying casts within a specified position/time/cruise tolerance

range, so any casts with matching position/time values within 0.001° and 12 hours were considered to be the same cast and merged.

Pressure inversions were found in some profiles. It occurs when an observation has a shallower depth than the observation directly preceding it. All profiles presenting pressure inversion in the whole cast were discarded.

Range checks were used to screen the data for extreme values using literature-based broad ranges for each variable (Boyer et al., 2019; Levitus & Boyer, 1994). These ranges for a given variable, in each region, is set large enough to encompass variations for all seasons and years at that oceanic basin (Boyer et al., 2019; Levitus & Boyer, 1994). Observed level data were compared with these ranges, and outliers were flagged and masked out. These ranges do not represent the minimum and maximum values in the basins, but rather indicate the extent of values beyond which the data are believed to be erroneous.

Obvious erroneous discrete data, entire casts, or even whole cruises have been flagged or excluded from analysis if judged to be doubtful or outside the large T-S ranges mentioned above. Furthermore, profiles were also considered unreliable if presented with less than 50 discrete measurements, noisy temperature/salinity values, or any error while importing into ODV. From the WOD18 and GLODAPv2.2020 datasets, data classified as questionable or bad quality were rejected from the analysis.

After the application of the QC, the total number of T-S profiles ready to be used throughout METAREA V was 4027, including both the BNDO and ancillary (WOD18 & GLODAPv2.2020) datasets merged.

2.3 Framework Analysis

The framework analysis is a matrix-based method widely used for analyzing qualitative data, developed during the 1980s at the National Centre for Social Research (Ritchie and Spencer, 1994). Since the 'thematic framework' is a central component of the method, such as in other analytic tools, it is indeed used to classify and organize data according to key themes, concepts, and emergent categories, facilitating rigorous and transparent data management (Ritchie & Lewis, 2014).

From the method perspective, each study will present a distinct thematic framework comprising a series of main themes, subdivided by a succession of related subtopics, which herein encompasses oceanographic cruises, data management, and analysis of the thermohaline structure. These steps unfold and are refined through familiarization with the raw data and cross-sectional labeling. Once it is judged to be comprehensive, i.e. after preprocessing and QC steps, each instance of analysis is synthesized and displayed/charted in its specific terms, according to the appropriate parts of the thematic framework (Ritchie & Lewis, 2014).

In the analysis stage, the gathered data is sifted, sorted, and charted. This involves a five-step process (Ritchie & Spencer, 1994): (i) familiarization; (ii) identifying a thematic framework; (iii) indexing; (iv) charting; (v) mapping and interpretation.

Thus, the method supplies a far-sight of the objectives of qualitative analysis for the researcher, which are: "defining concepts, mapping range and nature of phenomena, creating typologies, finding associations, providing explanations, and developing strategies" (Ritchie and Spencer, 1994:186).

The quality checked data were thus indexed and organized for further investigation and analysis through charting and mapping the salinity variability over the South Atlantic.

Several neutral density values were defined to assess the salinity variability over time, according to each section, as shown before in Table 2. For the Tropical section, profiles were used to assess absolute salinity along the following neutral density surfaces, respective to each water mass boundary (Herrford et al., 2017; Hummels et al., 2015): TW-SACW γ_n = 24.5 kg/m^3; SACW - AAIW γ_n = 26.8 kg/m^3; AAIW - NADW γ_n = 27.7 kg/m^3; NADW - AABW γ_n = 28.135 kg/m^3. For the Subtropical section, profiles were employed to determine absolute salinity at the same water mass interfaces, but with slightly different neutral density values, as shown in Table 2 (Azar et al., 2020; Goes et al., 2014; and Preu et al., 2012): TW-SACW γ_n = 26.2 kg/m^3; SACW - AAIW γ_n = 27.1 kg/m^3; AAIW - NADW γ_n = 27.6 kg/m^3; NADW - AABW γ_n = 28.10 kg/m^3.

The aforementioned novel and ancillary datasets were merged and employed to generate trend graphs and isosurface maps of Absolute Salinity for each defined neutral density layer via the Data-Interpolating Variational Analysis (DIVA) gridding technique, using automatic scale lengths and a signal-to-noise ratio of 50, while hiding bad estimates with a quality limit of 3, and excluding outliers. DIVA is a software tool, also coupled to ODV, developed for spatial interpolation of oceanographic in situ data, which has highly optimized calculations that rely on a finite element resolution considering coastlines, sub-basins, and advection (Troupin et al., 2012). The salinity variability trends were calculated for each layer using the least-square line fit over time from 1998 to 2018.

Many studies have sought to examine oceanographic circulation features; however, it is the combined spatial and temporal variability acting upon hydrographic properties which, together, determine the primary distribution of conservative tracers. This characteristic of ocean circulation is well demonstrated by the distribution of salinity along neutral density surfaces.

3. RESULTS AND DISCUSSION

Herein, after the preprocessing and quality check steps, 783 profiles (40%) of 28 cruises from the BNDO dataset have passed all tests and were considered reliable to be analyzed, out of a total of 1952 raw profiles during 39 cruises (Table 3). From those, 453 profiles were located within the Tropical section against 330 profiles in the Subtropical section. On the other hand, for the ancillary dataset (international repositories WOD18 & GLODAPv2.2020) used as a reference, 3244 profiles were gathered of which 2175 of them were located within the Tropical section and 1069 profiles in the Subtropical section.

Table 3. Metadata and number of raw/reliable stations of each oceanographic cruise incorporated in the BNDO dataset.

Oceanographic Cruise	Year	Austral Season	Section	Original Number of Profiles (NP)	NP after QC	% Reliable Profiles
PIRATA-BR 01	1998	Summer	Tropical	17	0	0
PIRATA-BR 02	1999	Summer	Tropical	32	23	72
Oceano Sudeste I	2000	Autumn/Winter	Subtropical	116	0	0
PIRATA-BR 03	2000	Summer	Tropical	21	19	90
Oceano Leste I	2001	Spring	Tropical/Subtropical	117	79	68
Oceano Norte I	2001	Winter	Tropical	146	0	0
PIRATA-BR 04	2001	Autumn	Tropical	25	24	96
Oceano Nordeste I	2002	Summer	Tropical	57	0	0
Oceano Sudeste II	2002	Spring	Subtropical	100	0	0
Oceano Sul I	2002	Winter	Subtropical	77	0	0
PIRATA-BR 05	2002	Autumn	Tropical	20	0	0
Oceano Sudeste III	2003	Spring	Subtropical	76	41	54
PIRATA-BR 06	2003	Winter	Tropical	20	19	95
Oceano Nordeste II	2004	Spring	Tropical	12	0	0
PIRATA-BR 07	2004	Winter	Tropical	5	5	100
Oceano Leste II	2005	Summer	Tropical/Subtropical	44	0	0
Oceano Norte II	2005	Spring	Tropical	23	14	61
PIRATA-BR 08	2005	Winter	Tropical/Subtropical	8	7	88
Costa Leste I	2006	Spring	Tropical	29	12	41
Oceano Sudeste IV	2006	Summer/Autumn	Subtropical	63	22	35
PIRATA-BR 09	2006	Spring	Tropical	27	24	89
Oceano Sul III	2007	Autumn	Subtropical	98	61	62
Oceano Norte III	2008	Spring	Tropical	26	17	65
PIRATA-BR 10	2008	Autumn	Tropical/Subtropical	27	14	52
Costa Nordeste I	2009	Winter	Tropical	114	19	17

Oceano Norte IV	2009	Winter	Tropical	30	15	50
Oceano Sul IV	2009	Spring	Subtropical	46	33	72
PIRATA-BR 11	2009	Summer/Autumn	Tropical/Subtropical	9	8	89
Oceano Sudeste V	2010	Winter	Subtropical	37	16	43
PIRATA-BR 12	2010	Winter	Tropical/Subtropical	34	34	100
Costa Sul III	2011	Summer/Autumn	Subtropical	107	59	55
PIRATA-BR 13	2011	Winter/Spring	Tropical/Subtropical	33	32	97
Oceano Leste III	2012	Autumn/Winter	Subtropical	44	30	68
Costa Nordeste II	2013	Winter	Tropical	96	15	16
Oceano Leste IV	2013	Spring	Tropical/Subtropical	87	25	29
PIRATA-BR 14	2013	Autumn	Tropical	4	0	0
PIRATA-BR 17	2017	Summer	Tropical/Subtropical	61	52	85
PIRATA-BR 18	2018	Spring	Tropical/Subtropical	64	64	100
Total				**1952**	**783**	**40%**

Finally, the full merged dataset to be analyzed, including both the novel (BNDO) and ancillary (WOD18 & GLODAPv2.2020) repositories, presented 4027 profiles within METAREA V (1998 - 2018) divided into 2583 in the Tropical section and 1393 in the Subtropical section. Figure 3 illustrates the spatial and temporal distribution of oceanographic stations used in this study.

Indeed, we focus on the mean vertical structure of the water column and the interannual variability of salinity as our time series are not long enough to investigate longer-term (for example decadal) scales, thus annual time series are detrended for statistical analysis as well as mean salinity climatologies are extracted for each neutral density layer previously defined. Kersalé et al. (2020) have shown that both the upper (more energetic) and abyssal cells of the Atlantic MOC exhibit significant variability at time scales between intraseasonal to annual periods, highlighting the necessity for a continuous-in-time trans-basin observing system, despite the longer-term variabilities that are not fully described with the available data.
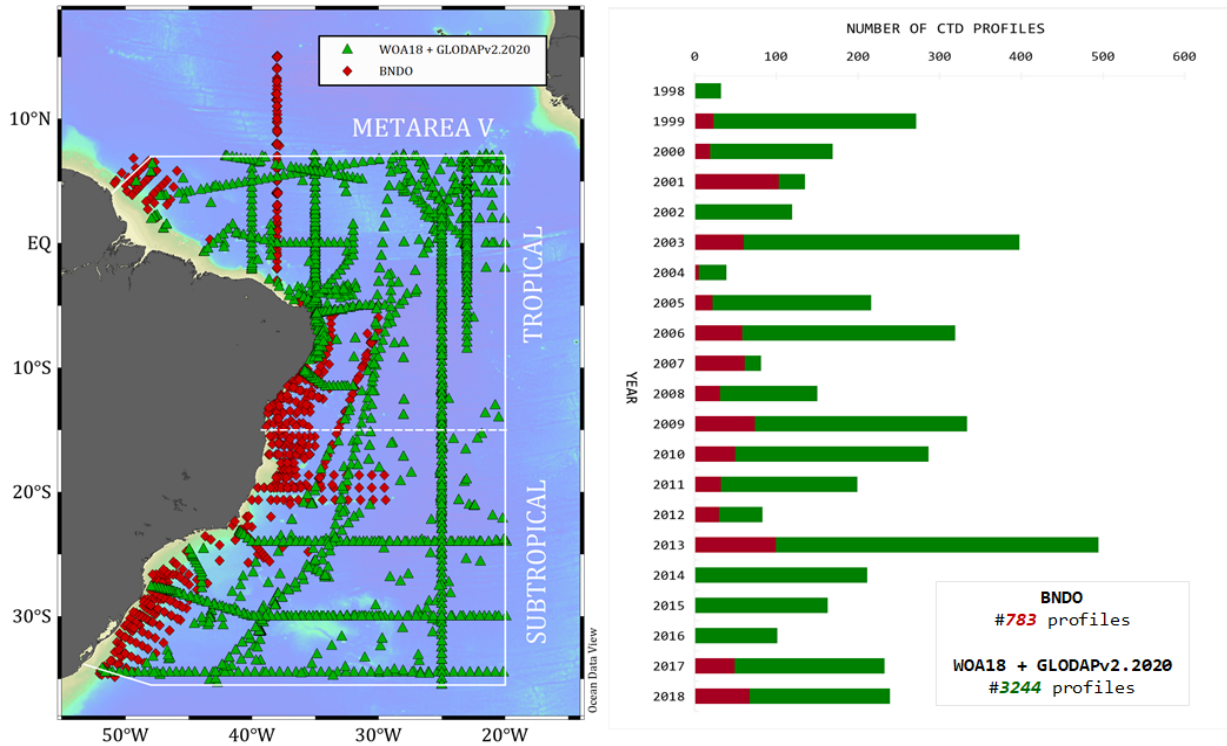
Figure 3. Left panel shows the spatial distribution of CTD profiles on each dataset, spanning from 1998 to 2018. Red diamonds depict this study dataset (BNDO) stations while green triangles represent the ancillary dataset (WOD18 & GLODAPv2.2020). White solid lines delimit METAREA V, while the dashed line depicts the division into Tropical and Subtropical sections at 15°S. Right panel shows the yearly distribution of profile casts for each dataset (same color scheme).

3.1. Vertical structure of the water column

Scatter profiles of each dataset were plotted for both Tropical and Subtropical sections, as illustrated in Figure 4, as well as the five major water masses identified in the profiles and indicated by their acronyms. Additionally, Figure 4 shows the benefit of assimilating the BNDO dataset in the main international repositories, e.g. WOD18 & GLODAPv2.2020, increasing the number of stations by 404 in the Tropical section (18.5% of 2583 available in that region), and by 328 in the Subtropical section (30.8% of 1393 available in that region). The presented novel dataset (BNDO) combined with ancillary data from

international repositories (WOD18 & GLODAPv2.2020) means a significant gain in spatio-temporal resolution of open-access ocean data.
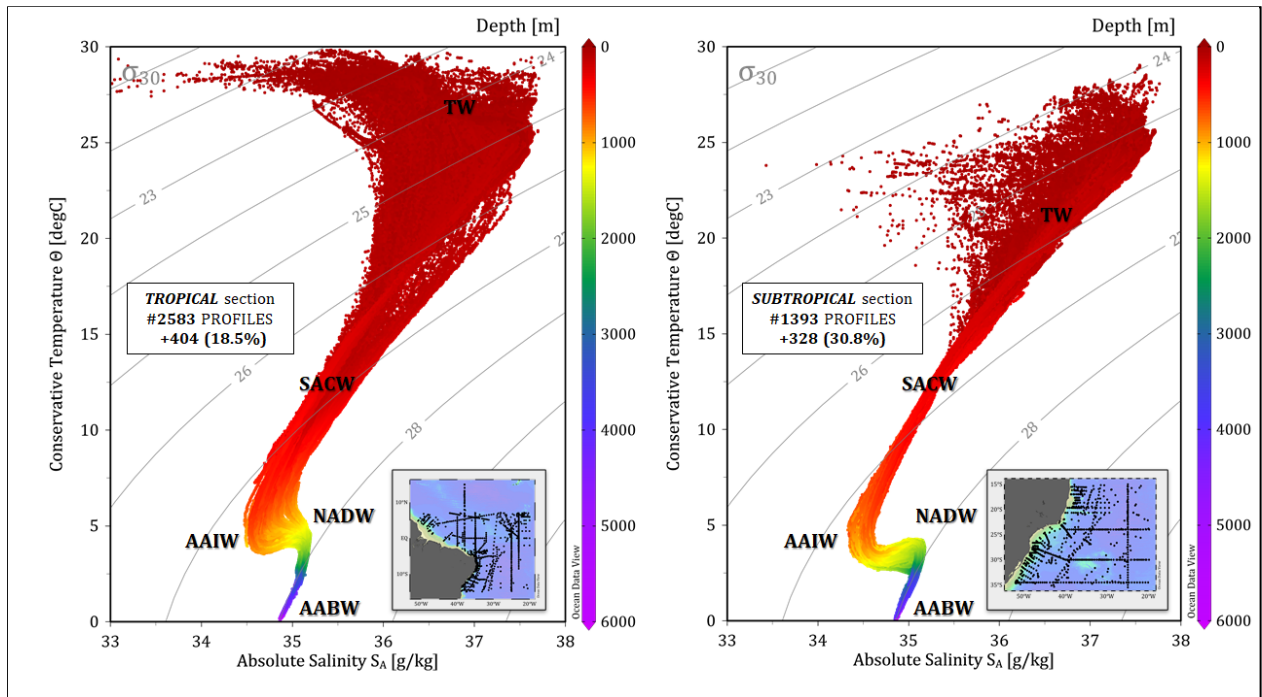

Figure 4. Scatter plots of Conservative Temperature, Absolute Salinity, and Depth (in color) for the Tropical (left panel) and Subtropical (right panel) Atlantic sections of this study dataset (BNDO + WOD18 + GLODAPv2.2020), spanning from the year of 1998 to 2018. The five major water masses identified are indicated by its acronyms while isopycnals are shown in grey lines and were plotted using a reference pressure of 30 dbar (σ_{30}).

At the sea surface, salinity is generally lower in the tropics and southernmost segments of the subtropical gyres than in the majority of the subtropics. Adjacent to the top of the thermocline, salinity reaches an acute subsurface maximum at depths of about 100-200 m, arising from high salinity surface waters in each subtropical gyre. This high salinity water subducts and flows equatorward and downward beneath the fresher, warmer TW, thus forming a salinity maximum layer (Talley, 2011).

As mentioned above, in the subtropics, salinity is high at the surface due to subtropical higher net evaporation if compared to the tropics. Then, salinity decreases to a minimum at depths of 600-1000 m (AAIW). Below this, salinity increases to a maximum

25

(NADW), with some variability of these exact depths of the vertical minimum and maximum depending on the ocean. In the Atlantic and Indian Oceans, the salinity maximum is at depths of 1500-2000 m (Talley, 2011).

At intermediate depths (1000-1500 m), there are horizontally extensive, vertically broad layers of either low salinity or high salinity. AAIW originates in the Southern Ocean near South America and is found throughout the Southern Hemisphere and tropics, being identified as a salinity minimum at depths in a given T-S profile (Talley, 2011).

At the deep layer, waters exhibit salinity variations that print their source area attributes. Once the North Atlantic is the saltiest oceans at the surface, dense waters are formed and subducted, carrying a high salinity signature as they advance southward into the Southern Hemisphere, so these waters are identified as a salinity maximum at depths and conventionally called NADW. Dense waters formed in the Antarctic continental shelves are colder, fresher, and denser than North Atlantic dense waters, so they are found beneath waters of North Atlantic origin. Their movement northward into the Atlantic can be tracked through their lower salinity and higher densities, being referred to as AABW. The vertical juxtaposition of the salty NADW and fresher AABW is apparent in the South Atlantic vertical profiles section (Ferreira & Kerr, 2017; Talley, 2011). Table 1 summarizes hydrographic coefficients for each of those water masses.

3.2 Mean distribution and temporal evolution of salinity along neutral density surfaces

Salinity variations at all timescales are less well documented than temperature variations, once the temperature is more easily measured and salinity requires indirect measurements and proof samples to better estimates (laboratory salinometer). Annual

variations of surface salinity in the open ocean are less than 0.5 (Talley, 2011). Temporal salinity and temperature variations at a given location can be quite significant at large-scale fronts between waters of different properties and source regions. These fronts are sometimes termed water mass boundaries. The fronts move about their mean location, on weekly, seasonal, and longer timescales, which requires a full suite of multi-scale analyses for improved monitoring of temporal variability and external influences. The meandering of fronts and the development of eddies from different types of waters can also cause large salinity and temperature variations in a given area.

Here, several neutral density surfaces, defined for each Tropical and Subtropical sections of METAREA V according to the literature and the results presented here (Fig. 4), are used to represent water mass boundaries across the South Atlantic. For the major five water masses that can be identified (TW, SACW, AAIW, NADW, AABW), four neutral density layers are used to divide the water column at each respective interface (TW-SACW; SACW-AAIW; AAIW-NADW; NADW-AABW).

Interannual and long-term changes in basin-scale salinity are observed and are part of the documentation of climate change. Large-scale, coherent salinity changes over several decades have been documented (Levitus et al., 2005; Durack & Wijffels, 2010) and can be linked to large-scale changes in precipitation and evaporation that might be related to an overall warming of the atmosphere as well as dynamics of the cryosphere (Bindoff et al., 2007). Additionally, the seasonal cycle and interannual variability can also represent a source of bias, particularly in the South Atlantic where historical data largely exists for the austral summer only, dropping a lack of winter data right when atmospheric dynamics are more active forcing the upper column.

The following Table 4 summarizes mean salinity values, standard deviations, number of measurements used, range span, and trends per year for each neutral density surface in this

study dataset. Isosurface maps displaying the spatial distribution of salinity along neutral density surfaces are also exhibited and discussed below.

Table 4. Summary of statistics and trends for each water mass interface divided into Tropical and Subtropical sections.

	Absolute Salinity (g/kg)									
	TROPICAL					SUBTROPICAL				
	Mean	Std Dev	Points	Range	Trend (g/kg . yr^{-1})	Mean	Std Dev	Points	Range	Trend (g/kg . yr^{-1})
TW – SACW										
	γ_n = 24.5 kg/m³					γ_n = 26.2 kg/m³				
This Study	36.476	0.458	2371 +394 (20%)	35.131 - 37.669	+ 0.01993	35.934	0.122	1331 +297 (28.6%)	35.461 - 36.403	+ 0.00186
Ancillary Data	36.42	0.444	1977	35.131 - 37.639	+ 0.01956	35.923	0.127	1037	35.461 - 36.403	+ 0.00103
SACW – AAIW										
	γ_n = 26.8 kg/m³					γ_n = 27.1 kg/m³				
This Study	35.301	0.0709	2261 +324 (16.7%)	34.744 - 36.16	+ 0.00062	34.722	0.062	1121 +208 (22.7%)	34.317 - 34.954	- 0.00231
Ancillary Data	35.300	0.0854	1937	34.744 - 35.629	+ 0.00151	34.713	0.058	913	34.317 - 34.914	- 0.00232
AAIW – NADW										
	γ_n = 27.7 kg/m³					γ_n = 27.6 kg/m³				
This Study	34.899	0.0546	1769 +207 (13.2%)	34.489 - 35.819	- 0.00155	34.6	0.041	1037 +170 (19.6%)	34.525 - 34.788	+ 0.00042
Ancillary Data	34.903	0.0472	1562	34.489 - 35.092	- 0.00198	34.598	0.040	867	34.525 - 34.788	+ 0.0009
NADW – AABW										
	γ_n = 28.135 kg/m³					γ_n = 28.10 kg/m³				
This Study	35.061	0.0152	880 +78 (9.7%)	34.893 - 35.799	- 0.00043	35.062	0.025	776 +44 (6%)	34.950 - 35.111	- 0.0016
Ancillary Data	35.06	0.0175	802	34.893 - 35.095	- 0.00068	35.061	0.025	732	34.950 - 35.093	- 0.00016

3.2.1. TW - SACW

The assimilation of the novel BNDO dataset into ancillary data (WOD18 + GLODAPv2.2020) altogether increases the number of discrete measurements in this layer (TW - SACW) by 20% in the Tropical section (γ_n = 24.5 kg/m³), and by 28.6% in the Subtropical section (γ_n = 26.2 kg/m³), totalizing 691 new discrete measurements (Table 4). Calculated mean salinity and values range indicate the presence of waters from both TW and SACW mainly fluctuating from the surface to depths of 160 m in the Tropical section, and from 30 to 300 m in the Subtropical, both being highly susceptible to internal and external variability once comprehending the most energetic layer of the water column.

The DIVA gridded maps (Fig. 5) show a strong gradient of more saline waters adjacent to the northeastern Brazilian coast, right under the influence of North Brazil Current, which has a velocity core centered at 100 - 200 m (Silveira et al., 1994), if compared to areas under the Amazon/Orinoco freshwater discharge influence or open waters. Further south, a marked gradient is notably contiguous to the Brazil Current recirculation gyre and the Brazil/Malvinas Confluence Zone, with fresher waters within oceanic regions.

In this layer, salinification trends are observed with magnitudes of +0.01 g/kg . yr^{-1} in the Tropical region, and of +0.001 g/kg . yr^{-1} in the Subtropical section. Boyer et al. (2005) observed the same salinification trend at the upper layer, possibly related to warming and increased evaporation in the tropics as mentioned before. Zhu & Liu (2020), when analyzing observational and modeling data, have noted a salinity pile-up in the South Atlantic upper layers, remotely caused by the AMOC slowdown, with rates from 0.1 to 0.3 century^{-1}, coherent with values observed in this study.
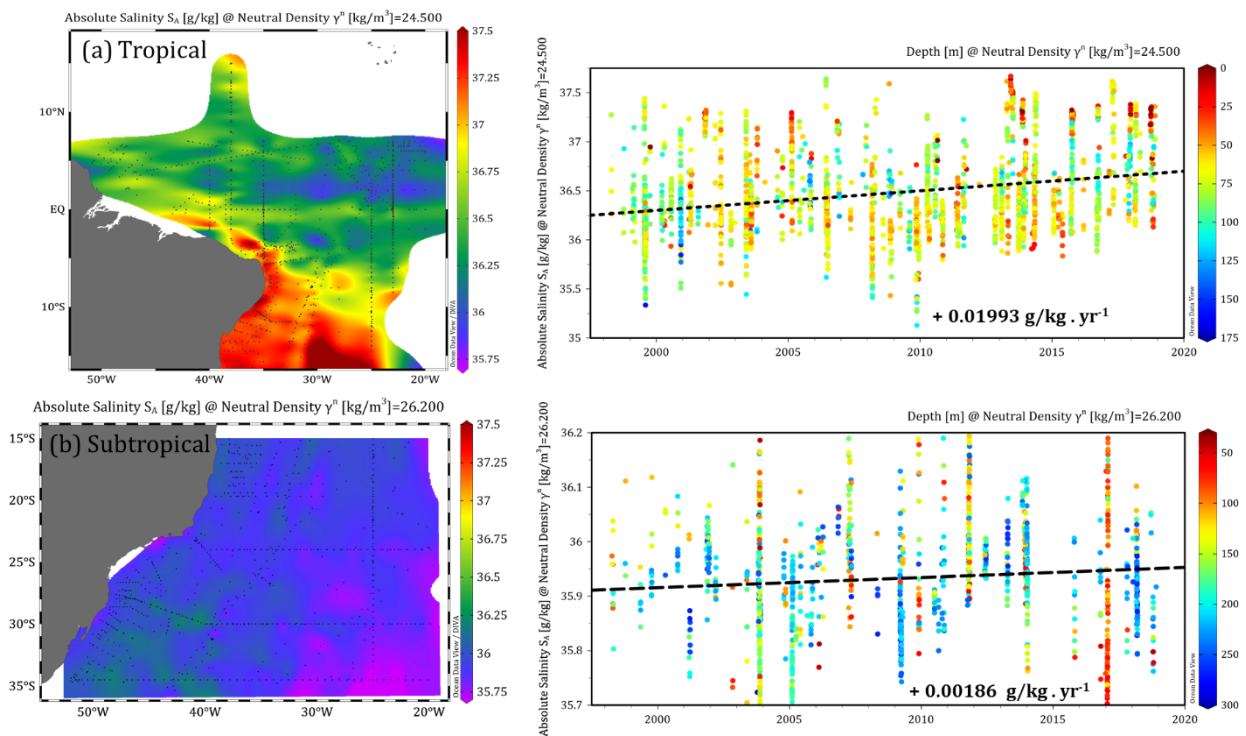
Figure 5. Left panels are plotted DIVA gridded maps of salinity measurements along the (a) γ_n = 24.5 kg/m^3 and (b) γ_n = 26.2 kg/m^3 neutral density layers, corresponding to the TW - SACW interface for both (a) Tropical and (b) Subtropical sections, respectively. Black dots mark station locations used as reference points for the gridding method. Right panels show the temporal evolution of salinity for the same scheme. Black dashed lines represent the linear fit of data points and the calculated annual trends (g/kg . yr^{-1}) are shown for each case. Colored dots display the depth of each discrete data.

3.2.2. SACW - AAIW

The assimilation of the novel BNDO dataset into ancillary data (WOD18 + GLODAPv2.2020) altogether raises the number of available data in this layer (SACW - AAIW) by 16.7% in the Tropical section (γ_n = 26.8), and by 22.7% in the Subtropical section (γ_n = 27.1), totalizing 532 new discrete measurements (Table 4). Calculated mean salinity and values range indicate the presence of waters from both SACW (more influence) and AAIW from about 100 to 800 m deep, mainly related to central and intermediate waters as expected. The DIVA gridded maps (Fig. 6) show three pronounced gradients: (i) between the North and South Atlantic basins waters, possibly related to the limits of SACW influence reaching up to 15°N (Stramma & England, 1999); (ii) accompanying the Vitoria-Trindade Ridge, with saltier waters in the northern portion, mostly related to a stronger influence of AAIW (fresher) southward; and (iii) near the Brazil-Malvinas Confluence, where SACW is formed (Stramma & England, 1999).

In this layer, annual salinification trends do not show a consensus between the Tropical and Subtropical sections. While the former presents a positive salinity variability in the order of +0.0006 g/kg . yr^{-1}, the latter presents a negative signal of -0.002 g/kg . yr^{-1} (Table 4).

Preceding studies (Curry et al., 2003; Goes et al., 2014; Yao et al., 2017) have found a basin-scale freshening of SACW and AAIW throughout the South Atlantic, which values are in accordance with our results for the Subtropical section.
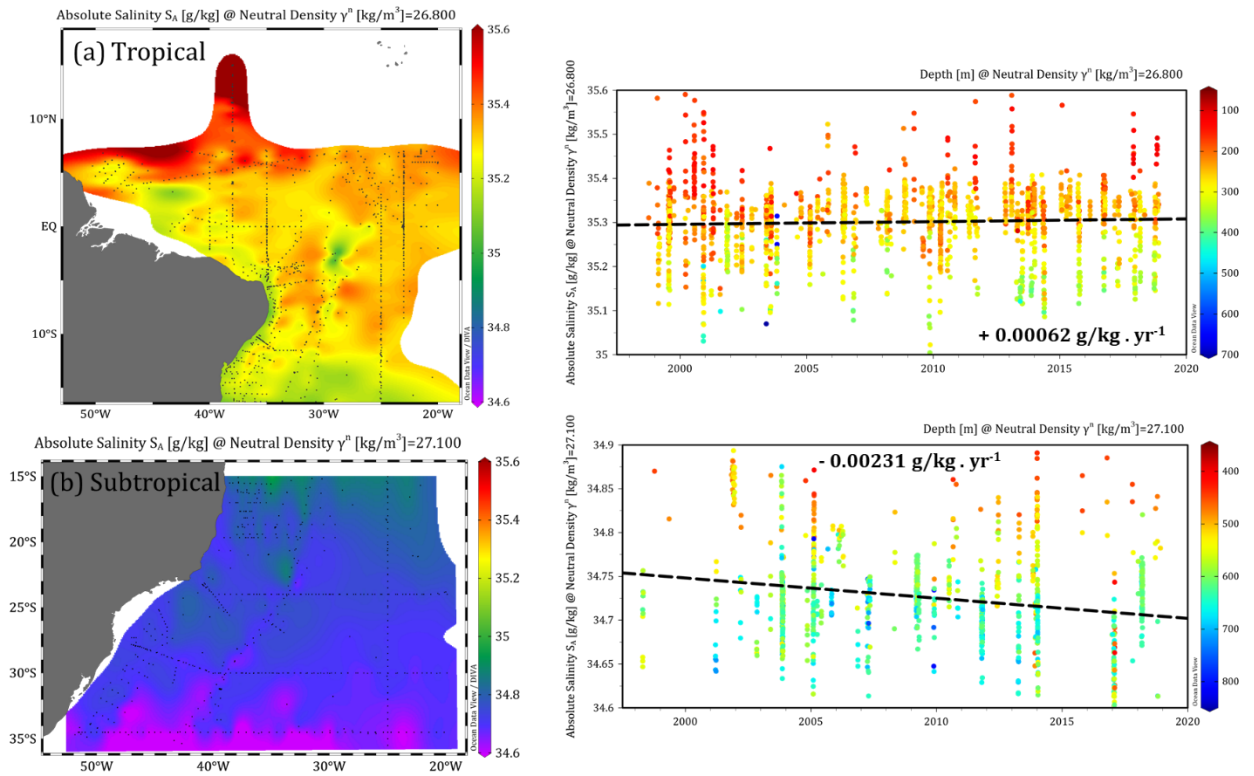
Figure 6. Left panels are plotted DIVA gridded maps of salinity measurements along the (a) γ_n = 26.8 kg/m^3 and (b) γ_n = 27.1 kg/m^3 neutral density layers, corresponding to the SACW - AAIW interface for both (a) Tropical and (b) Subtropical sections, respectively. Black dots mark station locations used as reference points for the gridding method. Right panels show the temporal evolution of salinity for the same scheme. Black dashed lines represent the linear fit of data points and the calculated annual trends (g/kg . yr^{-1}) are shown for each case. Colored dots display the depth of each discrete data.

3.2.3. AAIW - NADW

The assimilation of the novel BNDO dataset into ancillary data (WOD18 + GLODAPv2.2020) altogether raises the resolution of available data in this layer (AAIW - NADW) by 13.2% in the Tropical section (γ_n = 27.7), and by 19.6% in the Subtropical section (γ_n = 27.6), totalizing 377 new discrete measurements (Table 4). Calculated mean salinity and values range for this neutral density layer indicate the presence of waters from both AAIW and NADW, mainly at depths from 850 to 1400 m, related to intermediate and deep waters. The DIVA gridded maps (Fig. 7) display two notable gradients: (i) near the Equator, driven from a bigger influence of younger NADW (saltier) in the northernmost

portion while being under more influence of AAIW (fresher) to the south; and (ii) a latitudinal gradient near 25ºS, also related to the spatial distribution of NADW (saltier) and AAIW (fresher) percolation.

According to Reid (1989), the AAIW presence in the interior South Atlantic is limited to the subtropical gyre south of about 25°S and a northward flow of AAIW is found west of 20°W at 20°S, which concentrates near the Brazilian coast at about 15°S and recirculates in wide parts of the tropical South Atlantic. Other inverse calculations for sections at 7°30'N and 4°30'S show that the AAIW layer contributes water to the central water above as well as to the upper layer of the NADW below (Stramma & Schott, 1999). The AAIW core has a maximum pressure of ~900 dbar at 30°S before rising to 750 dbar around the equator (20°S–10°N) and deepening again in the North Atlantic (Schmidtko & Johnson, 2012). The AAIW core becomes denser in more northerly latitudes by entrainment and mixing, while in subtropical latitudes a zonal gradient of AAIW core density is distinguishable (Schmidtko & Johnson, 2012).

In this layer, interannual salinity variability trends do not show a consensus between Tropical and Subtropical sections and vary regionally in both sign and magnitude. While the former presents a negative salinity variability in the order of -0.001 g/kg . yr^{-1}, the latter presents a positive signal of +0.0004 g/kg . yr^{-1}. The AAIW salinity minimum influence persists to at least 20ºN, with northward spreading intensified at the western boundary in the subtropics (Schmidtko & Johnson, 2012).
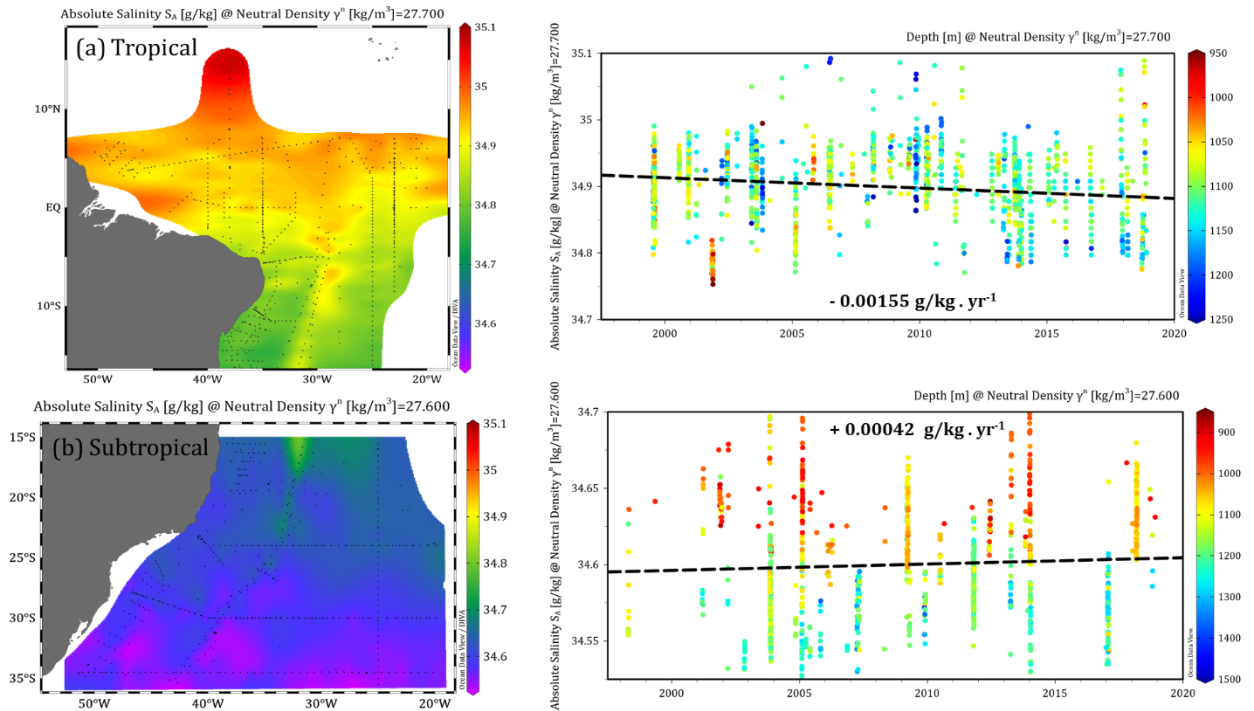
Figure 7. Left panels are plotted DIVA gridded maps of salinity measurements along the (a) γ_n = 27.7 kg/m^3 and (b) γ_n = 27.6 kg/m^3 neutral density layers, corresponding to the AAIW - NADW interface for both (a) Tropical and (b) Subtropical sections, respectively. Black dots mark station locations used as reference points for the gridding method. Right panels show the temporal evolution of salinity for the same scheme. Black dashed lines represent the linear fit of data points and the calculated annual trends (g/kg . yr^{-1}) are shown for each case. Colored dots display the depth of each discrete data.

3.2.4. NADW - AABW

The assimilation of the novel BNDO dataset into ancillary data (WOD18 + GLODAPv2.2020) altogether raises the resolution of available data in this layer (NADW - AABW) by 9.7% in the Tropical section (γ_n = 28.135), and by 6% in the Subtropical section (γ_n = 28.10), totalizing 122 new discrete measurements (Table 4). Calculated mean salinity and values range for this neutral density layer indicate the presence of waters from both NADW and AABW, mostly at depths from 2800 to 4600 m, related to deep and abyssal waters. The DIVA gridded maps (Fig. 8) display a cross-equatorial gradient, probably related to more NADW (saltier) influence in the northernmost portion while more influence of AABW (fresher) to the south, as well as a saltier tongue towards the South Atlantic basin

33

while fresher waters appear in the southernmost portion, likely a consequence of a stronger AABW intrusion.

Cold and dense Antarctic Bottom Water (AABW) forms at the Antarctic margin and feeds the abyssal layer of the global ocean, supplying the lower limb of the global overturning circulation, especially the Atlantic MOC. AABW occupies ~30–40% of the total volume of the global ocean and can store heat and carbon in the abyss for several centuries while its formation variability is inferred to regulate atmospheric carbon dioxide concentrations, and therefore the Earth's climate, on centennial to millennial timescales (Johnson, 2008).

The salinity, density and volume of AABW have decreased over the last 50 years, with the most marked changes observed in the Ross Sea (Silvano et al., 2020). These changes have been attributed to increased melting of the Antarctic Ice Sheet. In recent decades (70s to early 2010s) observations have shown that AABW has freshened by about 0.01 g . kg^{-1} per decade, which is in accordance with our results, and decreased in density while getting thinner (Jacobs et al., 2012).

The AABW fingerprint is transformed along its northward propagation, including into the South Atlantic. There are two causes of these salinity variations in AABW: (i) mixing with warmer and more saline layers of NADW; and (ii) geothermal heating (Frey et al., 2019). The flow of AABW to the north is generally concentrated in the abyssal Deep Western Boundary Current, which is striking in the Argentine Basin but becomes weaker in the Brazil Basin (Frey et al., 2019).

Antecedent works at the Antarctic Peninsula (Dotto et al., 2016; Abrahamsen et al., 2019) have compiled clear evidences that for at least the past fifty years, the AABW have shown significant trends of freshening and lightening, with impacts on their volume. The freshening signal may be forced by transformation of the water masses sourced in the

34

Weddell Sea continental shelf, possibly due to the melting of ice shelves and glaciers in the Antarctic Peninsula which reduces the salt flux into shelf waters, or could be related to a wind adjustment of the Weddell gyre which ultimately would heave the deep isopycnals favoring or not a younger less-mixed water.

In this layer, freshening trends are observed with magnitudes of -0.0004 g/kg . yr^{-1} in the Tropical section (γ_n = 28.135), and of -0.001 g/kg . yr^{-1} in the Subtropical (γ_n = 28.10). Despite data scarcity at such depths, the freshening annual trend corroborates with Purkey & Johnson (2013), Dotto et al. (2016), and Azaneu et al. (2013).
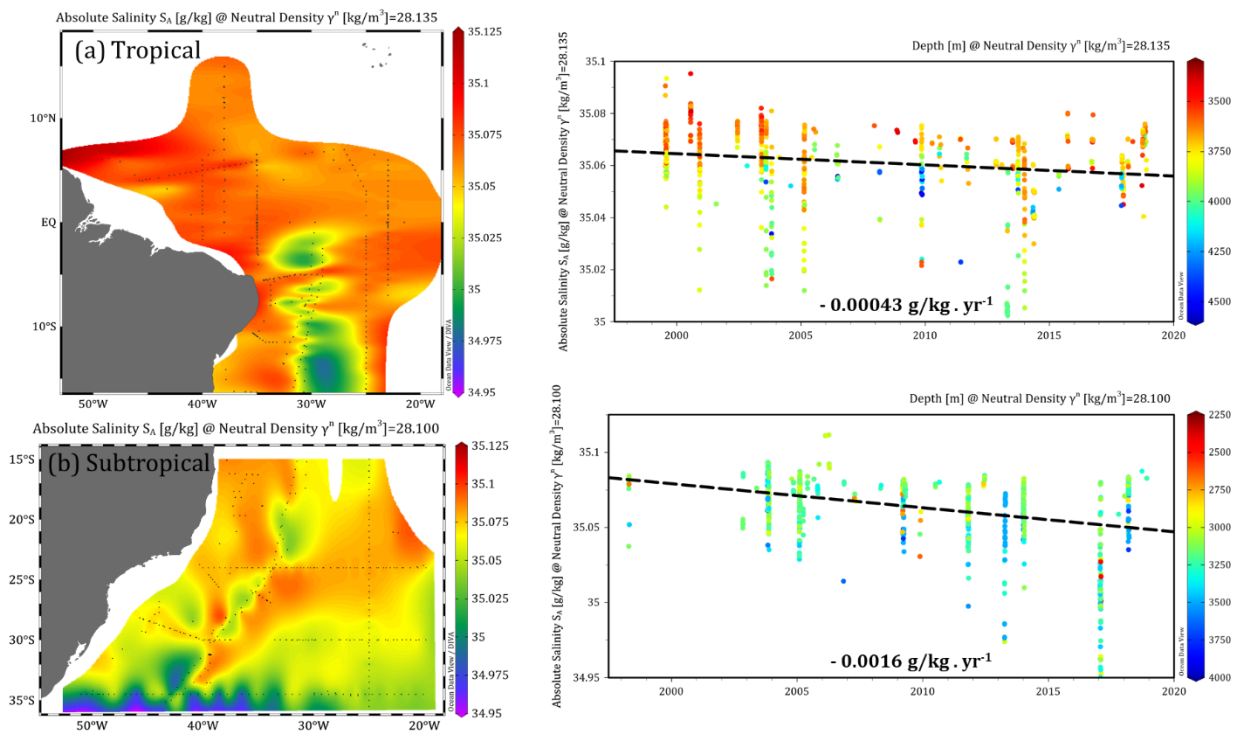
Figure 8. Left panels are plotted DIVA gridded maps of salinity measurements along the (a) γ_n = 28.135 kg/m^3 and (b) γ_n = 28.10 kg/m^3 neutral density layers, corresponding to the NADW - AABW interface for both (a) Tropical and (b) Subtropical sections, respectively. Black dots mark station locations used as reference points for the gridding method. Right panels show the temporal evolution of salinity for the same scheme. Black dashed lines represent the linear fit of data points and the calculated annual trends (g/kg . yr^{-1}) are shown for each case. Colored dots display the depth of each discrete data.

4. CONCLUSION

Monitoring changes and estimating trends in ocean circulation, as well as their consequences for the global heat and carbon budget, are still challenging even with recent progress on observational capabilities. Currents and water masses dynamics are highly variable on a large range of temporal and spatial scales. Synoptic sampling, such as GO-SHIP's hydrographic transects, can be combined with more frequent and bigger spatial coverage, such as remote sensing, drifters, and moorings arrays to better assess transport and velocity estimates. The integration of a full suite of available datasets has been crucial for better circulation analysis tools.

In this dissertation, salinity variability along neutral density layers of the Tropical and Subtropical Southwestern Atlantic is analyzed. The South Atlantic presents a well-marked depth-latitudinal dependent circulation with large-scale salinity inversions where the saline NADW is layered between the fresher AAIW and AABW. Three datasets were elected to construct a hydrographic review over two decades (1998-2018), including a novel one (BNDO) that was compared to both ancillary WOD18 and GLODAPv2.2020 datasets to assess its uniqueness. Then, the datasets were merged all together to investigate the vertical distribution of water masses and the temporal evolution of salinity.

The BNDO dataset has been used to improve the open-available ancillary data (WOD18 & GLODAPv2.2020) resolution. Results among the three datasets are coherent for general mean statistics and annual trends throughout the water column as a whole. To further advance the understanding of trends, interannual and interdecadal variation of hydrographic properties in the South Atlantic, it is essential to integrate distinct datasets from continuous discrete profiling, mooring arrays, drifters, and long-term observations, addressing the limitations of each method. The continuously improving data coverage allows insights into

water masses spreading and heat budget, as well as variability and trends of conservative temperature and absolute salinity.

There is still a clear need to enhance data management capacity, promote best practices in global common data standards and exchange protocols, as well as a plain vocabulary to ensure interoperability between datasets. The ocean data system architecture is incomplete and fragmented, and the revolution of free and open data sharing has yet many benefits to endorse (Tanhua et al., 2019).

Finally, the results are summarized in tables, charts and DIVA gridded maps of salinity along several neutral density surfaces. Despite a significant discard of profiles (60%) in the novel dataset, the qualified data (40%) presents full-depth high-resolution CTD profiles assessed within METAREA V, yet not fully integrated with the main international data repositories such as WOD and GLODAP. Hence, the incorporation of this novel dataset, as well as any other in a similar circumstance, would significantly enhance the spatio-temporal resolution of openly available data and better support future investigations in the South Atlantic, as demonstrated.

The results discussed here include salinification trends of +0.01993 g/kg . yr^{-1} (Tropical) and + 0.00186 g/kg . yr^{-1} (Subtropical) in upper waters, a dipole of freshening-salinification in central and intermediate waters, which presented +0.00062 g/kg . yr^{-1} and -0.00155 g/kg . yr^{-1} (Tropical SACW-AAIW and AAIW-NADW, respectively) in addition to -0.00231 . yr^{-1} and +0.00042 (Subtropical SACW-AAIW and AAIW-NADW, respectively), as well as a freshening of -0.00043 g/kg . yr^{-1} (Tropical) and -0.0016 g/kg . yr^{-1} (Subtropical) in deep and abyssal waters, mainly corroborating with precedent investigations through both observational and modeling methodologies, aside the gains in robustness and spatial data lacks over the Southwestern Atlantic.

Estimated trends outline how salinity changes over a given period, which in turn is determined by the data availability (1998-2018 in this study), so it could be not fully representative of a long-term trend, which remains questionable until existing databases develop enough for that. Nowadays, with ongoing and potentially accelerating trends related to anthropogenic climate and hydrological changes are constantly reported, decadal variabilities emerge as a valuable tool in ocean climatology assessment.

At last, the incorporation of other datasets such ARGO and ARGO-deep, as well as a statistics-focused analysis on these non-integrated datasets may reveal further important information for South Atlantic climatologies. The BNDO dataset compiled and employed herein is available upon request for the author at paivamatheus@id.uff.br and will also be uploaded to an online data repository for ready-access.

REFERENCES

Abrahamsen, E. P., Meijers, A. J. S., Polzin, K. L., Garabato, A. C. N., King, B. A., Firing, Y. L., Sallée, J-B., Sheen, K. L., Gordon, A. L., Huber, B. A., Meredith, M. P. (2019). Stabilization of dense Antarctic water supply to the Atlantic Ocean overturning circulation. Nature Climate Change, 9, 742-746. https://doi.org/10.1038/s41558-019-0561-2

Almeida, L., de Azevedo, J. L. L., Kerr, R., Araujo, M., & Mata, M. M. (2018). Impact of the new equation of state of seawater (TEOS-10) on the estimates of water mass mixture and meridional transport in the Atlantic Ocean. Progress in Oceanography, 162, 13–24. https://doi:10.1016/j.pocean.2018.02.008

Arbic, B. K. & Brechner Owens, W. (2001). Climatic warming of Atlantic intermediate waters. Journal of Climate, 14(20), 4091-4108. https://hdl.handle.net/2027.42/84360

Azaneu, M., Kerr, R., Mata, M. M., Garcia, C. A. E. (2013). Trends in the deep Southern Ocean (1958–2010): implications for Antarctic Bottom Water properties and volume export, J. Geophys. Res., 118, 4213–4227. https://doi.org/10.1002/jgrc.20303

Azar, E., Piñango, A., Wallner-Kersanach, M., & Kerr, R. (2020). Source waters contribution to the tropical Atlantic central layer: New insights on the Indo-Atlantic exchanges. Deep Sea Research Part I: Oceanographic Research Papers, 103450. https://doi.org/10.1016/j.dsr.2020.103450

Barberini, F. (2017). The Brazil Current and Intermediate Western Boundary Current Flows Through the Vitória-Trindade Ridge. https://hdl.handle.net/11422/6961

Barlett, R., E. M., Tosonotto, G. V., Piola, A. R., Sierra, M. E., & Mata, M. M. (2018). On the temporal variability of intermediate and deep waters in the Western Basin of the Bransfield Strait. Deep Sea Research Part II: Topical Studies in Oceanography, 149, 31–46. https://doi.org/10.1016/j.dsr2.2017.12.010

Belem, A. L., Caricchio, C., Albuquerque, A. L. S., Venancio, I. M., Zucchi, M. R., Santos, T. H. R., Alvarez, Y. G. (2019). Salinity and stable oxygen isotope relationship in the Southwestern Atlantic: constraints to paleoclimate reconstructions. Anais da Academia Brasileira de Ciências, 91(3), e20180226. Epub September 30, 2019. https://doi.org/10.1590/0001-3765201920180226

Bindoff, N. L. & Mcdougall, T. J. (1994). Diagnosing Climate Change and Ocean Ventilation Using Hydrographic Data. Journal of Physical Oceanography, 24(6), 1137–1152. https://doi.org/10.1175/1520-0485(1994)024<1137:DCCAOV>2.0.CO;2

Bindoff, N. L., Willebrand, J., Artale, V., Cazenave, A., Gregory, J. M., Gulev, S., Woodworth, P. (2007). Observations: oceanic climate change and sea level. In: Solomon, S.; Qin, D.; Manning, M.; Chen, Z.; Marquis, M.; Averyt, K.B.; Tignor, M.; Miller, H.L., (eds.) Climate change 2007: the physical science basis. Contribution of Working Group I. Cambridge, Cambridge University Press, 385-428. ISBN 9780521705967

Böning, C. W., Dispert, A., Visbeck, M., Rintoul, S. R., & Schwarzkopf, F. U. (2008). The response of the Antarctic Circumpolar Current to recent climate change. Nature Geoscience, 1(12), 864-869. https://doi.org/10.1038/ngeo362

Boyer, T. P., Levitus, S., Antonov, J. I., Locarnini, R. A., & Garcia, H. E. (2005). Linear trends in salinity for the World Ocean, 1955–1998. Geophysical Research Letters, 32(1). https://doi.org/10.1029/2004GL021791

Boyer, T. P., Baranova, O. K., Coleman, C., Garcia, H. E., Grodsky, A., Locarnini, R. A., Mishonov, A. V., Paver, C. R., Reagan, J. R., Seidov, D., Smolyar, I. V., Weathers, K. W., Zweng, M. M. (2019). World Ocean Database 2018. A. V. Mishonov, Technical Editor, NOAA Atlas NESDIS 87. https://www.ncei.noaa.gov/products/world-ocean-database

Bower, A., Lozier, S., Biastoch, A., Drouin, K., Foukal, N., Furey, H. (2019). Lagrangian views of the pathways of the Atlantic Meridional Overturning Circulation. Journal of Geophysical Research: Oceans, 124, 5313–5335. https://doi.org/10.1029/2019JC015014

Campos, E. J. D., Gonçalves, J. E., Ikeda, Y. (1995). Water mass characteristics and geostrophic circulation in the South Brazil Bight: Summer of 1991. Journal of Geophysical Research, 100(C9), 18537. https://doi:10.1029/95jc01724

Costa da Silva, A., Chaigneau, A., Dossa, A. N., Eldin, G., Araujo, M., Bertrand, A. (2021). Surface Circulation and Vertical Structure of Upper Ocean Variability Around Fernando de Noronha Archipelago and Rocas Atoll During Spring 2015 and Fall 2017. Frontiers in Marine Science, 8. https://doi.org/10.3389/fmars.2021.598101

Curry, R., Dickson, B., Yashayaev, I. (2003). A change in the freshwater balance of the Atlantic Ocean over the past four decades. Nature, 426(6968), 826–829. https://doi.org/10.1038/nature02206

Dorfschäfer, G. S., Tanajura, C. A. S., Costa, F. B., & Santana, R. C. (2020). A New Approach for Estimating Salinity in the Southwest Atlantic and Its Application in a Data Assimilation Evaluation Experiment. Journal of Geophysical Research: Oceans, 125(9). https://doi.org/10.1029/2020jc016428

Dotto, T. S., Kerr, R., Mata, M. M., Garcia, C. A. E. (2016). Multidecadal freshening and lightening in the deep waters of the Bransfield Strait, Antarctica, J. Geophys. Res. Oceans, 121. https://doi.org/10.1002/2015JC011228

Dotto, T. S., Mata, M. M., Kerr, R., & Garcia, C. A. E. (2021). A novel hydrographic gridded data set for the northern Antarctic Peninsula. Earth System Science Data, 13(2), 671–696. https://doi.org/10.5194/essd-13-671-2021

Durack, P. J., Wijffels, S. E. (2010). Fifty-year trends in global ocean salinities and their relationship to broad-scale warming. Journal of Climate, 23(16), 4342-4362. https://doi.org/10.1175/2010JCLI3377.1

Emery, W. J. (2001). Water Types and Water Masses. In Encyclopedia of Ocean Sciences (pp. 3179–3187). Elsevier. https://doi.org/10.1006/rwos.2001.0108

Ferreira, M. L. de C., Kerr, R. (2017). Source water distribution and quantification of North Atlantic Deep Water and Antarctic Bottom Water in the Atlantic Ocean. Progress in Oceanography, 153, 66–83. https://doi.org/10.1016/j.pocean.2017.04.003

Frey, D. I. Morozov, E. G., Ansorge, I., Fomin, V. V., Diansky, N. A., Tarakanov, R. Y. (2019). Thermohaline structure of Antarctic Bottom Water in the abyssal basins of the South Atlantic, Russ. J. Earth. Sci., 19, ES5005. https://doi.org/10.2205/2019ES000679

Fu, Y., Wang, C., Brandt, P., Greatbatch, R. J. (2019). Interannual variability of Antarctic Intermediate Water in the tropical North Atlantic. Journal of Geophysical Research: Oceans. https://doi.org/10.1029/2018jc014878

Garzoli, S. L., Dong, S., Fine, R., Meinen, C. S., Perez, R. C., Schmid, C., van Sebille, E., & Yao, Q. (2015). The fate of the Deep Western Boundary Current in the South Atlantic. Deep Sea Research Part I: Oceanographic Research Papers, 103, 125–136. https://doi.org/10.1016/j.dsr.2015.05.008

Goes, M., Wainer, I., Signorelli, N. (2014). Investigation of the causes of historical changes in the subsurface salinity minimum of the South Atlantic. Journal of Geophysical Research: Oceans, 119(9), 5654–5675. https://doi.org/10.1002/2014JC009812

Gourrion, J., Szekely, T., Killick, R., Owens, B., Reverdin, G., Chapron, B. (2020). Improved statistical method for quality control of hydrographic observations. Journal of Atmospheric and Oceanic Technology, 37(5), 789-806. https://doi.org/10.1175/JTECH-D-18-0244.1

Herrford, J., Brandt, P., Zenk, W. (2017). Property changes of deep and bottom waters in the Western Tropical Atlantic. Deep Sea Research Part I: Oceanographic Research Papers, 124, 103–125. https://doi.org/10.1016/j.dsr.2017.04.007

Hirschi, J., Marotzke, J. (2007). Reconstructing the meridional overturning circulation from boundary densities and the zonal Wind stress. Journal of Physical Oceanography. Vol. 37, 743 – 763, https://doi:10.1175/JPO3019.1

Hummels, R., Brandt, P., Dengler, M., Fischer, J., Araujo, M., Veleda, D., & Durgadoo, J. V. (2015). Interannual to decadal changes in the western boundary circulation in the Atlantic at 11°S. Geophysical Research Letters, 42(18), 7615–7622. https://doi.org/10.1002/2015GL065254

Iudicone, D., Madec, G., McDougall, T. J. (2008). Water-Mass Transformations in a Neutral Density Framework and the Key Role of Light Penetration. Journal of Physical Oceanography, 38(7), 1357–1376. https://doi.org/10.1175/2007jpo3464.1

Jackett, D. R., McDougall, T. J. (1997). A Neutral Density Variable for the World's Oceans. Journal of Physical Oceanography, 27(2), 237–263. https://doi.org/10.1175/1520-0485(1997)027<0237:ANDVFT>2.0.CO;2

Jacobs, S., Jenkins, A., Hellmer, H., Giulivi, C., Nitsche, F., Huber, B., Guerrero, R. (2012). The Amundsen Sea and the Antarctic Ice Sheet. Oceanography 25(3):154–163, http://doi.org/10.5670/oceanog.2012.90

Johnson, G. C., Schmidtko, S., Lyman, J. M. (2012). Relative contributions of temperature and salinity to seasonal mixed layer density changes and horizontal density gradients. Journal of Geophysical Research: Oceans, 117(C4). https://doi.org/10.1029/2011JC007651

Katsumata K, Nakano H, Kumamoto Y. 2015. Dissolved oxygen change and freshening of Antarctic Bottom water along 62∘S in the Australian-Antarctic Basin between 1995/1996 and 2012/2013. Deep-Sea Res. II 114:27–38. https://doi.org/10.1016/j.dsr2.2014.05.016

Kersalé, M., Meinen, C. S., Perez, R. C., Le Hénaff, M., Valla, D., Lamont, T., Sato, O. T., Dong, S., Terre, T., van Caspel, M., Chidichimo, M. P., van den Berg, M., Speich, S., Piola, A. R., Campos, E. J. D., Ansorge, I., Volkov, D. L., Lumpkin, R., Garzoli, S. L. (2020). Highly variable upper and abyssal overturning cells in the South Atlantic. Science Advances, 6(32), eaba7573. https://doi.org/10.1126/sciadv.aba7573

Koltermann, K. P., Gouretski, V., Jancke, K. (2011). Hydrographic Atlas of the World Ocean Circulation Experiment (WOCE): Volume 3: Atlantic Ocean. National Oceanography Centre. http://whp-atlas.ucsd.edu/atlantic/atlas_text/WHPAtlas_Vol3_Atlantic_Introduction.pdf

Levitus, S., Burgett, R., Boyer, T. P. (1994). World Ocean Atlas 1994. Volume 3. Salinity. National Environmental Satellite, Data, and Information Service, United States. Web. https://www.osti.gov/biblio/137202-world-ocean-atlas-volume-salinity

Levitus, S., Antonov, J. I., Boyer, T. P., Garcia, H. E., Locarnini, R. A. (2005). Linear trends of zonally averaged thermosteric, halosteric, and total steric sea level for individual ocean basins and the world ocean (1955–1959) − (1994–1998). Geophysical Research Letters, 32(16). https://doi.org/10.1029/2005GL023761

Marson, J. M., Wainer, I., Mata, M. M., Liu, Z. (2014). The impacts of deglacial meltwater forcing on the South Atlantic Ocean deep circulation since the Last Glacial Maximum. Climate of the Past, 10(5), 1723-1734. https://doi.org/10.5194/cp-10-1723-2014

McCarthy, G., McDonagh, E., King, B. (2011). Decadal Variability of Thermocline and Intermediate Waters at 24°S in the South Atlantic. Journal of Physical Oceanography, 41(1), 157–165. https://doi.org/10.1175/2010JPO4467.1

McDougall, T. J. (1987). Neutral surfaces in the ocean: Implications for modelling. Geophysical Research Letters, 14(8), 797–800. https://doi.org/10.1029/GL014i008p00797

McDougall, T. J., Feistel, R., Pawlowicz, R. (2013). Thermodynamics of Seawater. Ocean Circulation and Climate, Vol. 103. https://dx.doi.org/10.1016/B978-0-12-391851-2.00006-4

McTaggart, K., Johnson, G. (2010). Notes on Ctd/O2 Data Acquisition and Processing Using Sea-Bird Hardware and Software (As Available). In Cell. http://www.pmel.noaa.gov/pubs/PDF/mcta3534/mcta3534.pdf

Olsen, A., Lange, N., Key, R. M., Tanhua, T., Bittig, H. C., Kozyr, A., Àlvarez, M., Azetsu-Scott, K., Becker, S., Brown, P. J., Carter, B. R., Cotrim, L., Feely, R. A., van Heuven, S., Hoppema, M., Ishii, M., Jeansson, E., Jutterström, S., Landa, C. S., Lauvset, S. K., Michaelis, P., Murata, A., Pérez, F. F., Pfeil, B., Schirnick, C., Steinfeldt, R., Suzuki, T., Tilbrook, B., Velo, A., Wanninkhof, R., Woosley, R. J. (2020). GLODAPv2.2020 − the second update of GLODAPv2. https://doi.org/10.5194/essd-2020-165

Palmer, M. D., Durack, P. J., Chidichimo, M. P., Church, J. A., Cravatte, S., Hill, K., Johannessen, J. A., Karstensen, J., Lee, T., Legler, D., Mazloff, M., Oka, E., Purkey, S., Rabe, B., Sallée, J.-B., Sloyan, B. M., Speich, S., von Schuckmann, K., Willis, J., Wijffels, S. (2019). Adequacy of the Ocean Observation System for Quantifying Regional Heat and Freshwater Storage and Change. Frontiers in Marine Science, 6. https://doi.org/10.3389/fmars.2019.00416

Pawlowicz, R. (2010). What every oceanographer needs to know about TEOS-10 (The TEOS-10 Primer). Unpublished manuscript. https://www.TEOS-10.org

Poole, R., Tomczak, M. (1999). Optimum multiparameter analysis of the water mass structure in the Atlantic Ocean thermocline. Deep Sea Research Part I: Oceanographic Research Papers, 46(11), 1895–1921. https://doi.org/10.1016/S0967-0637(99)00025-4

Preu, B., Schwenk, T., Hernández-Molina, F. J., Violante, R., Paterlini, M., Krastel, S., Tomasini, J., Spieß, V. (2012). Sedimentary growth pattern on the northern Argentine slope: The impact of North Atlantic Deep Water on southern hemisphere slope architecture. Marine Geology, 329–331, 113–125. https://doi.org/10.1016/j.margeo.2012.09.009

Rayner, D., Hirsch, J.J.M., Kanzow, T., Johns, W.E., Wright, P.G. (2011). Monitoring the Atlantic meridional overturning circulation. Deep-Sea Research II (58) 1744-1753. https://doi:10.1016/j.dsr2.2010.10.056

Reid, J.L. (1989). On the total geostrophic circulation of the South Atlantic Ocean: flow patterns, tracers and transports. Progress in Oceanography 23, 149—244. https://doi.org/10.1016/0079-6611(94)90014-0

Ritchie, J., Lewis, J. (2014). Qualitative research practice: A guide for social science students and researchers. London: SAGE Publications.

Schlitzer, R. (2018). Ocean Data View. https://odv.awi.de

Schmidtko, S., Johnson, G. C. (2012). Multidecadal Warming and Shoaling of Antarctic Intermediate Water, Journal of Climate, 25(1), 207-221. https://journals.ametsoc.org/view/journals/clim/25/1/jcli-d-11-00021.1.xml

Schott, F. A., Dengler, M., Zantopp, R., Stramma, L., Fischer, J., Brandt, P. (2005). The Shallow and Deep Western Boundary Circulation of the South Atlantic at 5°−11°S. Journal of Physical Oceanography, 35(11), 2031–2053. https://doi.org/10.1175/JPO2813.1

Sea-Bird Scientific (2017). Seasoft V2: SBE Data Processing - CTD Data Processing & Plotting Software for Windows. Software Manual. https://www.seabird.com/asset-get.download.jsa?code=251446

Silvano, A., Foppert, A., Rintoul, S. R., Holland, P. R., Tamura, T., Kimura, N., Macdonald, A. M. (2020). Recent recovery of Antarctic Bottom Water formation in the Ross Sea driven by climate anomalies. Nature Geoscience. https://doi.org/10.1038/s41561-020-00655-3

Silveira, I. C., de Miranda, L. B., Brown, W. S. (1994). On the origins of the North Brazil Current. Journal of Geophysical Research: Oceans, 99(C11), 22501-22512. https://doi.org/10.1029/94jc01776

Sloyan, B. M., Wanninkhof, R., Kramp, M., Johnson, G. C., Talley, L. D., Tanhua, T., Campos, E. (2019). The global ocean ship-based hydrographic investigations program (GO-SHIP): a platform for integrated multidisciplinary ocean science. Frontiers in Marine Science, 6, 445. https://doi.org/10.3389/fmars.2019.00445

Souza, A. G. Q. de, Kerr, R., Azevedo, J. L. L. de. (2018). On the influence of Subtropical Mode Water on the South Atlantic Ocean. Journal of Marine Systems, 185, 13–24. https://doi.org/10.1016/j.jmarsys.2018.04.006

Srivastava, A., Thomson, S. B. (2009). Framework Analysis: A Qualitative Methodology for Applied Research Note Policy Research. JOAAG, Vol. 4. No. 2. http://research.apc.org/images/a/ad/Framework_analysis.pdf

Stammer, D., Martins, M. S., Köhler, J., Köhl, A. (2020). How good do we know ocean salinity and its changes? Progress in Oceanography (2020). https://doi.org/10.1016/j.pocean.2020.102478

Stramma, L., England, M. (1999). On the water masses and mean circulation of the South Atlantic Ocean. In Journal of Geophysical Research: Oceans (Vol. 104, Issue C9, pp. 20863–20883). https://doi.org/10.1029/1999JC900139

Stramma, L., Schott, F. (1999). The mean flow field of the tropical Atlantic Ocean. Deep Sea Research Part II: Topical Studies in Oceanography, 46(1-2), 279–303. https://doi:10.1016/s0967-0645(98)00109-x

Swift J. H., Orsi A. H. (2012). Sixty-four days of hydrography and storms: RVIB Nathaniel B. Palmer's 2011 S04P Cruise. Oceanography 25(3):54–55. https://doi.org/10.5670/oceanog.2012.74

Talley, L. D. (2008). Freshwater transport estimates and the global overturning circulation: shallow, deep and throughflow components. Progress in Oceanography. 78:257–303. https://doi.org/10.1016/j.pocean.2008.05.001

Talley, L. D., Pickard, G. L., Emery, W. J., Swift, J. H. (2011). Descriptive physical oceanography: An introduction: Sixth edition. In Descriptive Physical Oceanography: An Introduction: Sixth Edition. Elsevier. https://doi.org/10.1016/C2009-0-24322-4

Talley, L. D., Feely, R. A., Sloyan, B. M., Wanninkhof, R., Baringer, M. O., Bullister, J. L., Zhang, J.-Z. (2016). Changes in Ocean Heat, Carbon Content, and Ventilation: A Review of the First Decade of GO-SHIP Global Repeat Hydrography. Annual Review of Marine Science, 8(1), 185–215. https://doi.org/10.1146/annurev-marine-052915-100829

Tanhua, T., McCurdy, A., Fischer, A., Appeltans, W., Bax, N., Currie, K., Wilkin, J. (2019). What We Have Learned From the Framework for Ocean Observing: Evolution of the Global Ocean Observing System. Frontiers in Marine Science, 6. https://doi:10.3389/fmars.2019.00471

Troupin, C., Barth, A., Sirjacobs, D., Ouberdous, M., Brankart, J. M., Brasseur, P., Rixen, M., Alvera-Azcárate, A., Belounis, M., Capet, A., Lenartz, F., Toussaint, M. E., and Beckers, J. M (2012). Generation of analysis and consistent error fields using the Data Interpolating Variational Analysis (DIVA), Ocean Model., 52–53, 90-101. https://www.researchgate.net/publication/258687663_Generation_of_analysis_and_consistent_error_fields_using_the_Data_Interpolating_Variational_Analysis_DIVA

Todd, R. E., Chavez, F. P., Clayton, S., CRAVATTE, S. E., Goes, M. P., Graco, M. I., Lin, X., Sprintall, J., Zilberman, N. V., Archer, M., Arístegui, J., Balmaseda, M. A., Bane, J. M., Baringer, M. O., Barth, J. A., Beal, L. M., Brandt, P., Calil, P. H., Campos, E., … Zhang, L. (2019). Global perspectives on observing ocean boundary current systems. Frontiers in Marine Science, 6(JUL). https://doi.org/10.3389/fmars.2019.00423

Tziperman, Eli. (1986). On the role of interior mixing and air-sea fluxes in determining the stratification and circulation of the oceans. Journal of Physical Oceanography 16(4): 680-693. https://doi.org/10.1175/1520-0485(1986)016%3C0680:OTROIM%3E2.0.CO;2

Urbano, D. F., Jochum, M., da Silveira, I. C. A. (2006). Rediscovering the second core of the Atlantic NECC. Ocean Modelling, 12(1-2), 1–15. https://doi:10.1016/j.ocemod.2005.04.003

Yao, W., Shi, J., Zhao, X. (2017). Freshening of Antarctic Intermediate Water in the South Atlantic Ocean in 2005–2014. Ocean Science, 13(4), 521–530. https://doi.org/10.5194/os-13-521-2017

Zhu, C., Liu, Z. (2020). Weakening Atlantic overturning circulation causes South Atlantic salinity pile-up. Nature Climate Change. https://doi.org/10.1038/s41558-020-0897-7